Analytical design model of coil parameters for the electro-magnetic forming technology - Case of the 1-turn coil dedicated to tubular parts forming and crimping with 1D approximation

Olivier Maloberti, Omar Mansouri, Denis Jouaffre, Mohammed Hamzaoui, Jimmy Derosiere, Nicolas Buiron, Pascal Sansen, Thaneshan Sapanathan, Philippe Pelca, Mohamed Rachik, et al.

Analytical Design Model of Coil Parameters for the Electro-Magnetic Forming Technology – *Case of the 1-Turn coil dedicated to tubular parts forming and crimping with 1D approximation*

MALOBERTI Olivier[a,b,1], MANSOURI Omar[a], JOUAFFRE Denis[c], HAMZAOUI Mohammed[d], DEROSIERE Jimmy[e], BUIRON Nicolas[f], SANSEN Pascal[a], SAPANATHAN Thaneshan[f], PELCA Philippe[g], RACHIK Mohamed[f], LEONARD Jean-Paul[h], LEMBROUCK Gregory[e], HAYE Dominique[c], MACRET Antoine[h].

[a]*ESIEE Amiens, Ecole Supérieure des Ingénieurs en Electrotechnique et Electronique, 14 quai de la Somme, 80080 cedex 2 Amiens, France*
[b]*LPSC-UPJV, Laboratoire de Physique des Systèmes Complexes, Université Picardie Jules Verne, 33 rue Saint Leu, 80039 Amiens cedex, France*
[c]*PFT-Innovaltech, Plateforme Technologique Innovaltech, Rond-point Frédéric Joliot-Curie, 02100 Saint-Quentin, France*
[d]*LTI-UPJV, Laboratoire des Technologies Innovantes, Université de Picardie Jules Verne, INSSET 48 rue d'Ostende CS10422, 02315 St-Quentin, France*
[e]*BASIS EP, 164 rue de la Chaussée Romaine, 02100 Saint-Quentin, France*
[f]*Roberval-UTC, Laboratoire Roberval, Centre de recherche de Royallieu, Université Technologique de Compiègne, CS 60319, 60203 Compiègne, France*
[g]*Le Bronze Alloys, Etablissement de Bornel, 11 rue du Ménillet BORNEL, 60540 Méru, France*
[h]*INDUXIAL, 64 Rue Hoche, 80300 Albert, France*

Keywords

Magnetic pulse technology
Magnetic pulse forming, crimping and welding
Physical modelling
Electromagnetism in matter
Bessel and approximation functions
Analytical design and calculation methods
Magnetic energy and inductance
Electrical loss and resistance
Electromagnetic Lorentz force

Abstract

In this paper, we propose an analytical electromagnetic modelling and an electromechanical coupling of the 1-turn bulk coil with a cut, made of conducting steel or copper alloys, and used in the electro-magnetic forming technology. The electromagnetic part of the work is the one created beyond the state of the art. Such analytical models that can quickly solve for key process parameters are extremely desirable but must be completed with a mechanical model able to calculate in the end the deformation. An existing mechanical model to calculate the deformation is used and coupled to our electromagnetic model. First, the basic electromagnetic theory will be summarised and then the One-Dimensional (1-D) axi-symmetrical approximation discussed (part 2). The goal is to be able to determine the magnetic vector potential $\boldsymbol{A}$ diffusion, that will quickly lead to all the parameters needed to characterize, qualify, feed and optimize the use of the coil (ex.: magnetic flux density, equivalent inductance, force coefficients, …). Then the pseudo-harmonic solution of the 1D-problem is expanded with the help of Bessel basis functions, including some specific limit conditions and constraints (part 3). The results are compared to numerical 2-D and 3-D computations, performed, thanks to the Finite Element Method, onto some test cases without and with a tube to deform. The proposed model does not only give the numerical value of each parameter, but it provides analytical formulae, with explicit dependences upon some key geometrical and physical variables (ex.: changeable air-gap between the coil and the tube linked to the deformation). The use of a pseudo harmonic working condition will be justified by comparing it to the transient working condition for which the model is improved. Experimental measurements will be carried out with and without a tube but with no deformation (part 4). The results are close and coherent and useful when sizing the coil with respect to performance criteria and performing an equivalent electrical circuit and an electro-mechanical coupling solution, usable with deformation in the transient working conditions (part 5).

[1]: corresponding author Olivier MALOBERTI (maloberti@esiee-amiens.fr, olivie.maloberti@gmail.com)

1. Introduction and context

Electromagnetic problems in Electrical Engineering are usually divided into three categories: low, intermediate and high frequencies. At low frequencies, quasi-static conditions prevail over transient ones and the classical resistance, as well as the inductance value of a component, do not depend on the frequency. At high frequencies, wave equations are used to predict the propagation of electromagnetic waves. Both these regions have been studied extensively. The magnetic pulse technology, that benefits from the Lorentz force effects produced in a metal by the pulsed magnetic field, fall into this intermediate frequency region, where eddy currents take place. Different geometries of inductors are investigated to generate electromagnetic pulses. Psyk et al. (2011) introduced several industrial cases for which the single-turn coil (see **Figure 1**) is often preferable to the multi-turn coil because it is more robust and simple. Most of electromagnetic models compatible with the tube compression with a single-turn coil do not provide any prediction on the actual current and flux densities distribution within conducting regions. For example, Nassiri et al. (2015) does not give details on these densities that are just said to penetrate homogeneously inside a very classical cartesian skin depth. The resulting magnetic field is calculated thank to the Biot and Savart law, only for the enforced current. In fact then, current source must be known. The same problem occurs for the resistance or the inductance calculation. Kinsey and Nassiri (2017) gives estimations without taking the actual current distribution inside the materials into account. Finally, the Lorentz force density should also be highly influenced by the eddy currents radial distribution either in the tube (deformation expected) or in the coil (deformation and cracking to avoid), which is not recently described neither by most authors on this subject nor by weddeling et al. (2015), whose main contribution is rather on the mechanical behavior. In the pulsed magnetic technology, we must compute not only the single-turn coils each carrying a known current source; we must calculate the natural eddy currents and skin effects in the coil, in the field-shaper and in the tube. Therefore, the total current source densities are not primarily known and must be calculated. This led us look for other past contributions to adapt calculations to this new technology.

Thus, the aim is first the inclusion of the skin effect into electrical parameters (resistance, inductance, force coefficients) within cylindrical coordinates, then the evaluation of the electromagnetic fields, densities and force, and finally the prediction of the deformation and of the process global efficiency. This paper proposes an analytical method to calculate the electromagnetic fields and densities that are generated by the current pulse in an inductor, as used in the magneto-forming technology. Two versions of the model will be investigated to avoid any misleading assumption and make sure each induced current is effectively and correctly calculated. Its usefulness will be emphasized by coupling it with electrical and mechanical models to allow deformation and efficiency predictions.

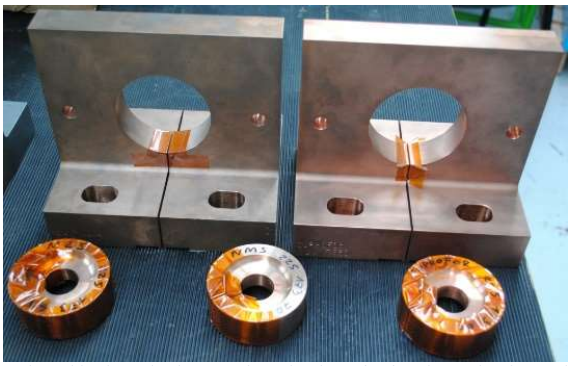

Figure 1. The single turn coil modelled and used in the pulsed magnetic technology for forming, crimping and welding processes @PFT Innovaltech.

We suggest studying one single turn coil example made of a conducting massive coil. Due to a cut within the toroidal coil between the two terminals, the geometry is strictly speaking a 3D component with no axial symmetry. Sapanathan et al. (2015) studied the mechanical behaviour of the single-turn coil and the tube with a 3D numerical method. Because this cut is very small and due to a big computation time, we, Maloberti et al. (2015), would like to investigate the possibility to reduce this geometry into an equivalent 2D and then 1D axi-symmetrical model, to give a good approximate solution. Guglielmetti (2012) studied the electromagnetic and mechanical behaviour of a cylindrical multi-turn coil and a tube with a 2D numerical method. For our purpose, Dodd (1967) provided the basis of the solutions to electromagnetic induction problems. Mansouri et al. (2016) introduced an analytical method to describe the electromagnetic behaviour of the single-turn coil dedicated to the magneto-forming process without a tube. The coil is highly conducting and the source always delivers a sinusoidal pulse varying very quickly in time with a natural frequency f_n (typically from 1 to 100 kHz) and an exponential

decay. We suggest computing the model with time harmonics in order to analyse the eddy currents, skin effects and induced Lorentz forces either in the coil, in the field-shaper or in the tube. In the following, we will first derive the general 1D Partial Differential Equation (PDE) in cylindrical coordinates, then solve the problem in the harmonic working condition, and finally give the main electromagnetic fields, densities, and parameters.

2. Theoretical preliminaries

2.1. The general physical equations

The equations for the magnetic vector potential $\boldsymbol{A}$ can be derived from the Maxwell's equations, involving the magnetic field $\boldsymbol{H}$, the flux density $\boldsymbol{B}$, the current density $\boldsymbol{j}$, the electric field $\boldsymbol{E}$ and the electronic displacement field $\boldsymbol{D}$. The media are assumed to be linear, isotropic and homogeneous: $\boldsymbol{B}=\mu\boldsymbol{H}$, $\boldsymbol{D}=\varepsilon\boldsymbol{E}$, $\boldsymbol{j}=\sigma\boldsymbol{E}$. μ and ε are respectively the absolute magnetic permeability and dielectric permittivity. σ is the electric conductivity. According to Dodd and Deeds (1968), the conduction ($\sigma\boldsymbol{E}$) is much greater than the propagation ($\partial(\varepsilon\boldsymbol{E})/\partial t$), so the latter may be neglected for frequencies below about ten megacycles per second. The magnetic induction field $\boldsymbol{B}$ is expressed as the curl of a magnetic vector potential $\boldsymbol{A_i}$. The coil is driven by a voltage generator with an applied voltage ΔV. The total electric field $\boldsymbol{E}$ is thus the sum of the source field $\boldsymbol{E}_s=-\nabla(V)$ and the induced field $\boldsymbol{E}_i=-\partial_t\boldsymbol{A}_i$, where V *is* an electric scalar potential. In the following, we investigate the possibility of looking at either a total magnetic potential $\boldsymbol{A}$ (Eq. (1), (3)), responsible for the total electric field $\boldsymbol{E}$, or a reduced magnetic vector potential $\boldsymbol{A_i}$ (Eq. (2), (4)), responsible for the induced field $\boldsymbol{E_i}$. Both lead to the total electric current density $\boldsymbol{j}$, including enforced and induced currents, such that (∇ is the *Nabla* operator, "∧" is the cross product, "." is the dot product):

$$\boldsymbol{E}=-\frac{\partial \boldsymbol{A}}{\partial t},\ \boldsymbol{j}=\sigma\boldsymbol{E}\ \text{with}\ \boldsymbol{B}=\nabla\wedge\boldsymbol{A}\quad(1);\quad \boldsymbol{E}=-\frac{\partial \boldsymbol{A_i}}{\partial t}-\nabla(V),\ \boldsymbol{j}=\sigma\boldsymbol{E}\ \text{with}\ \boldsymbol{B}=\nabla\wedge\boldsymbol{A_i}\quad(2)$$

By using the Coulomb gauge also used by Maloberti et al. (2015) $\nabla\boldsymbol{A}=0$ or $\nabla\boldsymbol{A_i}=0$, the Maxwell equations give for $\boldsymbol{A}$ and $\boldsymbol{A_i}$:

$$\Delta\boldsymbol{A}-\mu\sigma\frac{\partial \boldsymbol{A}}{\partial t}=0\quad(3);\quad \Delta\boldsymbol{A_i}-\mu\sigma\frac{\partial \boldsymbol{A_i}}{\partial t}=+\mu\sigma\nabla(V)\quad(4)$$

2.2. 2D and 1D geometrical assumptions

Figure 2 shows the inductor in 3, 2 and 1 dimensions respectively. In 1D axial symmetric models only the θ (orthoradial) components A_θ and j_θ are present in the magnetic vector potentials $\boldsymbol{A}$ and $\boldsymbol{A_i}$ and in the current density $\boldsymbol{j}$. Then, we obtain the homogeneous and non-homogeneous Partial Differential Equations (PDE) (5) and (6) of the inductor in cylindrical coordinates (r,θ,z). It is written as a function of $A(r,t)=A_\theta(r,t)$ or $A_i(r,t)=A_{i\theta}(r,t)$, depending on the radius r and time t, while neglecting both the z and θ dependences.

$$\frac{\partial^2 A}{\partial r^2}+\frac{1}{r}\frac{\partial A}{\partial r}-\frac{A}{r^2}-\mu\sigma\frac{\partial A}{\partial t}=0\quad(5);\quad \frac{\partial^2 A_i}{\partial r^2}+\frac{1}{r}\frac{\partial A_i}{\partial r}-\frac{A_i}{r^2}-\mu\sigma\frac{\partial A_i}{\partial t}=+\mu\sigma\frac{\partial V}{r\partial\theta}\quad(6)$$

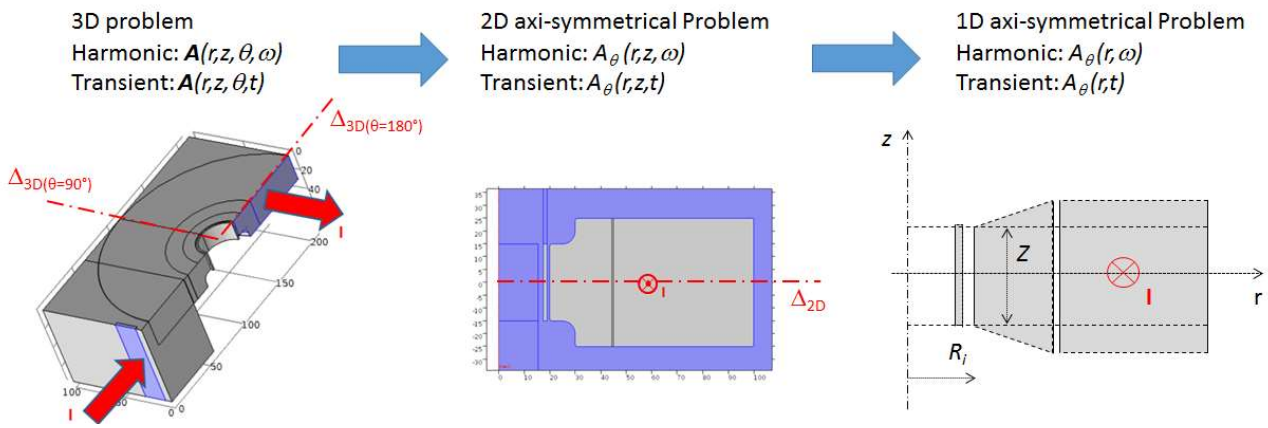

Figure 2. Geometry of the 3D geometry and its reduced models.

2.3. 3D effects considerations and limitations

The model will be calculated in one dimension (1D) for which the useful length Z of the inductor should be "quasi-infinite". We suggest comparing the analytical results to 2D numerical simulations obtained with the Finite Element method, that have been already compared to 3D calculations and measurements by Maloberti et al. (2015). The discrepancy between results is mainly due to the finite Z dependence of the actual fields and densities. In order to reduce this error, we must take the length Z into account. In the 2D numerical simulations, we can observe that the current density j is expanding with a longer effective length $Z_c=(Z+2\Delta Z)$, including the edges at both sides of the region c (c=1, 3 or 5 for the coil, 1 for the tube, 3 for the field-shaper) (**Figure 3**). In conclusion, we propose the use of Z_c instead of Z in the model. The absolute and relative difference $2\Delta Z$ between Z_c and Z can be expressed and estimated as a function of the internal radius R_i and the actual length Z of region c as follows (for large enough length such that $(R_i/Z) \leq 3\ \%$, it tends towards zero):

$$if\left(\frac{R_i}{Z}\right)>\frac{2}{100},\frac{\Delta Z}{Z}=\frac{Z_c-Z}{2Z}\approx\sum_{k=2}^{k=4}a_k I_{\frac{1}{k}}\left(\frac{1}{2}\left(\frac{R_i}{Z}\right)\right) \qquad (7)$$

$$a_2\approx 0.940; a_3\approx 1.689; a_4\approx -1.383$$

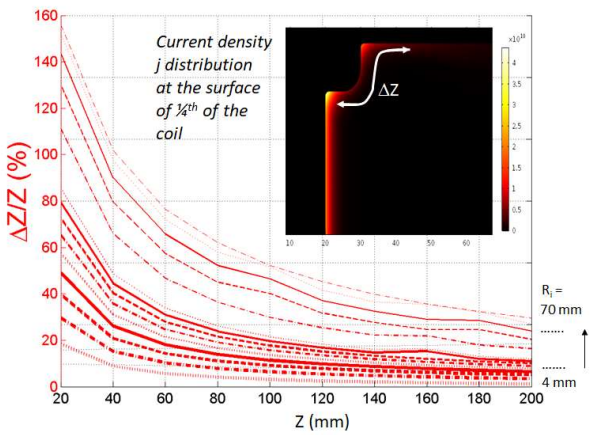

Figure 3. Calculation of the ΔZ correction length according to the length Z of inductor for different values of R_i [4,6,8,10,12,14,16,18,20,30,40,50,60,70].

The exponents and coefficients of the fitting function have been adjusted with respect to the 2D computations given by Maloberti et al. (2015). The first analysis consists in adjusting the value of ΔZ for various R_i ([4;70] mm) and Z ([20;200] mm), in order to fit the 2D numerical data. We observe that ΔZ depends mainly on the ratio between the radius R_i and Z, but the relative error $\Delta Z/Z$ is rapidly decreasing while the length is increasing, thus rendering the 1D assumption more relevant (**Figure 3**). The 1D hypothesis stays reliable if Z is very large compared to R_i $((R_i/Z) \leq 3\ \%)$ or providing the correction length ΔZ given by Eq. (7). The modified Bessel functions of the 1st kind of order $1/k$ ($I_{1/k}$) have been chosen to rely on the natural base functions of the quasi-static 1D and the 2D solutions studied by several authors. Conway (2001) found the exact solution of the magnetic field in axi-symmetrical solenoids, but providing that the current source distribution is known and simple. Labinac et al. (2006) calculated the magnetic fields of cylindrical coils due to a known surface current and a volume current in a cylindrical coil. Ravaud et al. (2010) derived the mutual inductance and force exerted between thick coils carrying uniform current volume densities. Unfortunately, the current source densities cannot be primarily known and must be calculated. The present paper gives a solution with 1D approximations for which the 2D effect is given by Eq. (7). This last impediment is not completely satisfactory. It will however be less time consuming and easier to perform any sensitivity analysis to the whole parameters, optimisation or coupling procedures with an analytical model. Another limitation may come from the dependence of such a 2D factor on the conductivity and the permeability. We observe that it is more sensitive to the geometry (ratio between the radius and the length) than to the physical properties σ and μ, which fix the skin depth (taken into account in the model).

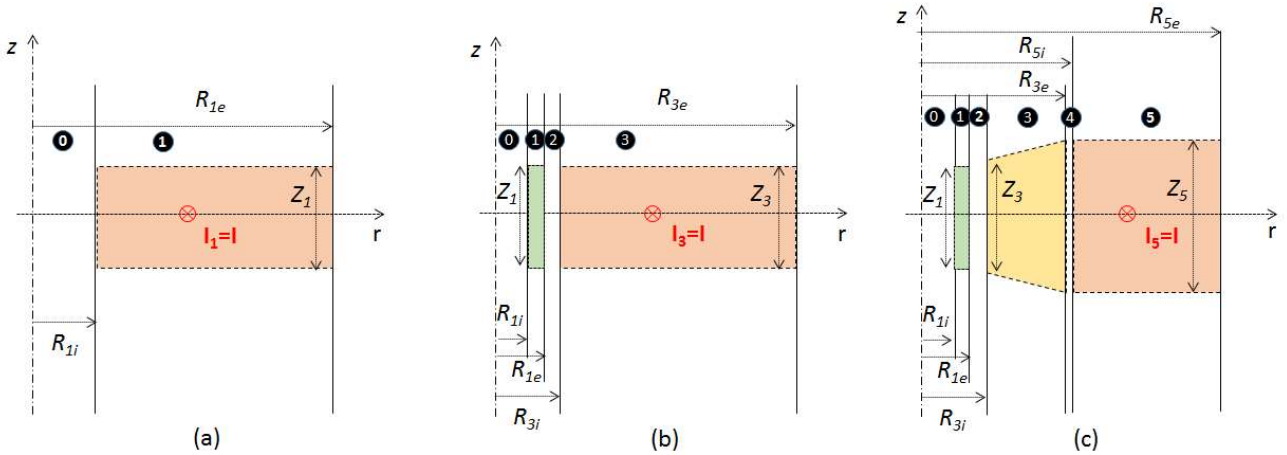

Figure 4. Domains Geometry of the 1D reduced models, without field-shaper nor tube (**a**), without field-shaper but tube (**b**), with field-shaper and tube (**c**)

3. The 1D magneto-harmonic model

Assuming that both the voltage V and the total current I are sinusoidal functions of time, $\Delta V(t) = \Delta V e^{i\omega t+\varphi}$ and $I(t) \equiv Ie^{i\omega t}$, then A is likewise a sinusoidal function of time, $A_\theta = Ae^{i\omega t}$, with A being the complex magnitude. Equation (5) is therefore written as follows:

$$\frac{\partial^2 A}{\partial r^2}+\frac{1}{r}\frac{\partial A}{\partial r}-\frac{A}{r^2}-i\omega\mu\sigma A=0 \qquad (8);\quad \frac{\partial^2 A_i}{\partial r^2}+\frac{1}{r}\frac{\partial A_i}{\partial r}-\frac{A_i}{r^2}-i\omega\mu\sigma A_i=\mu\sigma\frac{\Delta V}{2\pi r} \qquad (9)$$

In such a 1D axial symmetric model, if only the θ (orthoradial) component $A_\theta(r,\omega)$ is present in the magnetic potential $\boldsymbol{A}=A(r,\omega)\boldsymbol{u_\theta}$, it can easily be shown that $\boldsymbol{E}$, $\boldsymbol{j}$, $\boldsymbol{H}$ and $\boldsymbol{B}$ have also got only one component: $\boldsymbol{E}=E(r,\omega)\boldsymbol{u_\theta}$, $\boldsymbol{j}=j(r,\omega)\boldsymbol{u_\theta}$, $\boldsymbol{H}=H(r,\omega)\boldsymbol{u_z}$ and $\boldsymbol{B}=B(r,\omega)\boldsymbol{u_z}$.

3.1. General solution of the homogeneous PDE with the total magnetic vector potential A

3.1.1. Conducting regions

We consider that the total current density is included in the magnetic potential equation. For this, the 1D PDE in the harmonic working condition is given by Eq. (10) (ω is the angle velocity of the current, $\alpha^2 = \mu\sigma\omega$). Eq. (8) or (9) are known as the modified Bessel equations well introduced, detailed and solved by Gray and Mathews (1985) with the Bessel functions for very general problems and by Figueiredo and Laks (1989) with the Kelvin functions for similar magnetic cylinders. Then our solution is built and given by Eq. (11) or (12).

$$r^2\frac{\partial^2 A}{\partial r^2}+r\frac{\partial A}{\partial r}-(1+ir^2\alpha^2)A=0 \qquad (10)$$

$$A(r,\omega)=C'J_1(\alpha_1 r)-i*D'K_1(\alpha_2 r) \qquad (11)$$

$$A(r,\omega)=CJ_1(\alpha_1 r)+DY_1(\alpha_1 r) \qquad (12)$$

With $\alpha_1=\alpha.\exp(3\pi i/4)$ and $\alpha_2=\alpha.exp(\pi i/4)$ ($\alpha_1^*=-\alpha_2$), and where J_1 is the 1st order and 1st kind Bessel function, for which the relevance is emphasized by Conway (2001) in the magnetic field and by Conway (2007) in the coil inductance, Y_1 is the 1st order and 2nd kind Bessel function (Neumann function) and K_1 is the 1st order and 2nd kind modified Bessel function ($K_1(x)=-(\pi/2)\big(J_1(ix)+iY_1(ix)\big)$). *C'* or *C* and *D'* or *D* come from boundary conditions on *H* and constraints on *j* (see next § and **Figure 5**).

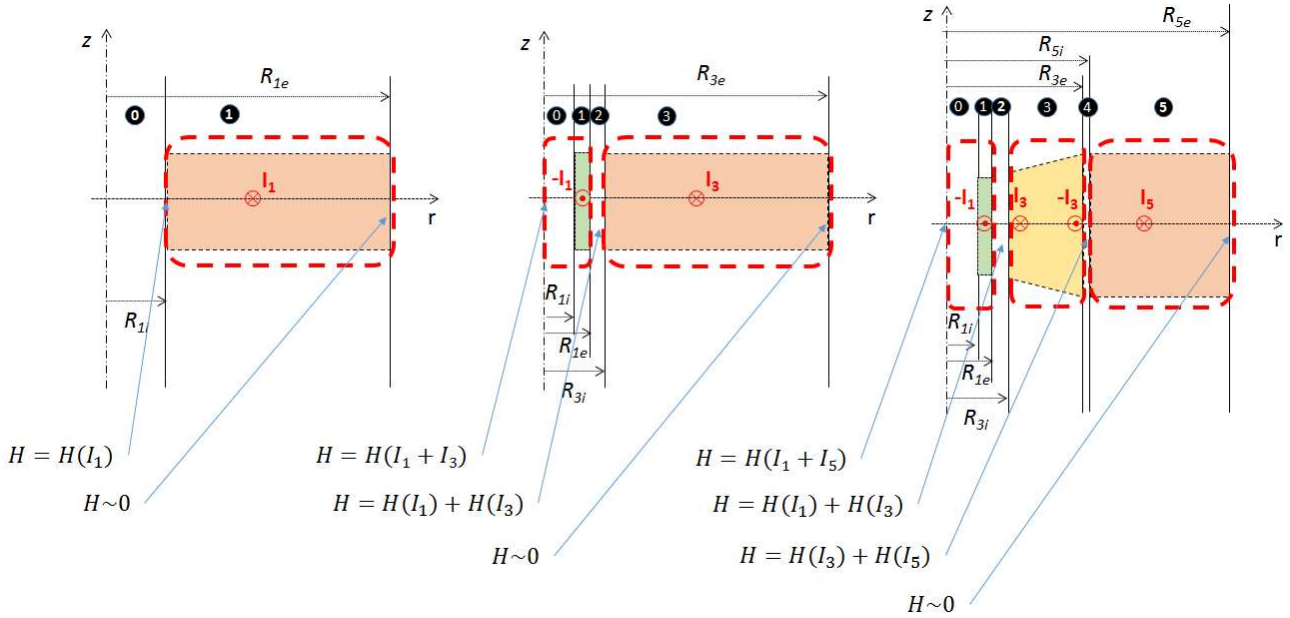

Figure 5. Constraints and limit conditions, with-no field-shaper and no tube (**a**), with field-shaper but no tube (**b**), with field-shaper and with tube (**c**).

3.1.2. Air and airgap regions

The 1D PDE in the air regions with neither conductivity nor current and its solution are shown in Equations (13) and (14).

$$r^2\frac{\partial^2 A}{\partial r^2}+r\frac{\partial A}{\partial r}-A=0 \qquad (13)\Leftrightarrow A(r)=Cr+D/r \qquad (14)$$

3.2. Complete solution of the total magnetic vector potential A as a function of the current I

In the following, we will consider conducting regions only, numbered 1, 3 and 5. As a consequence, previous solutions can be identified for each region with its number in index. All the following solutions are given in the Appendix B.1. after some mathematical operations.

3.2.1. Inductor without field-shaper nor tube

This case corresponds to case (a) of **Figure 4** and **Figure 5**. Only one conducting region is considered, the bulk 1-turn coil.

We now need a limit condition on the surface magnetic field H, and a constraint on the total current density j, and we assume that the inductor has a finite equivalent corrected length Z_l along the z axis (even if no z dependence is considered, see § 2.3). Equation (15) comes from the current conservation principle inside the coil section and equation (16) comes from the Maxwell-Ampere theorem applied onto the external limit of the coil section. It means that the flux of the current density j and the circulation of the magnetic field H equal the current $I_l=I$ in region 1 (the coil).

$$I = \int_{R_{1i}}^{R_{1e}} \int_{-Z_1/2}^{+Z_1/2} j dr dz = -\sigma_1 Z_1 i\omega \int_{R_{1i}}^{R_{1e}} A(r,\omega) dr \quad (15)$$

$$I = \oint H dl = H_z(R_{1i},\omega) Z_1 = \frac{Z_1}{\mu_1}\left(\frac{A(R_{1i},\omega)}{R_{1i}} + \partial_r A(R_{1i},\omega)\right) \quad (16)$$

Some mathematical operations give:

$$C_1 = \frac{[C_{11}Y_0(\alpha_1 R_{1i}) - D_{12}(Y_0(\alpha_1 R_{1e}) - Y_0(\alpha_1 R_{1i}))]}{[Y_0(\alpha_1 R_{1i})J_0(\alpha_1 R_{1e}) - Y_0(\alpha_1 R_{1e})J_0(\alpha_1 R_{1i})]} = K_{C1}\left(\frac{I}{Z}\right) \quad (17)$$

$$D_1 = \frac{[-C_{11}J_0(\alpha_1 R_{1i}) + D_{12}(J_0(\alpha_1 R_{1e}) - J_0(\alpha_1 R_{1i}))]}{[Y_0(\alpha_1 R_{1i})J_0(\alpha_1 R_{1e}) - Y_0(\alpha_1 R_{1e})J_0(\alpha_1 R_{1i})]} = K_{D1}\left(\frac{I}{Z}\right) \quad (18)$$

where: $C_{11} = \frac{\alpha_2}{\sigma_1 Z_1 \omega} I$ (19) and $D_{12} = \frac{\mu_1}{Z_1 \alpha_1} I$ (20)

The constants K_{C1} and K_{D1} only depend on the material properties (μ, σ), the geometry (R_i, R_e, Z) and the angle velocity ($\omega=2\pi f$). They are given in equations (21) and (22). The results show that the magnitude of the magnetic vector potential and its derivative quantities (the fields B, H and density j, see § 3.4) are proportional to the current per unit length (I/Z).

$$K_{C1} = \sqrt{\frac{\mu_1}{\sigma_1 \omega}}\left(\frac{Z}{Z_1}\right)\frac{\left[\left(\frac{\alpha_2}{\alpha}\right)Y_0(\alpha_1 R_{1i}) - \left(\frac{\alpha}{\alpha_1}\right)(Y_0(\alpha_1 R_{1e}) - Y_0(\alpha_1 R_{1i}))\right]}{[Y_0(\alpha_1 R_{1i})J_0(\alpha_1 R_{1e}) - Y_0(\alpha_1 R_{1e})J_0(\alpha_1 R_{1i})]} \quad (21)$$

$$K_{D1} = \sqrt{\frac{\mu_1}{\sigma_1 \omega}}\left(\frac{Z}{Z_1}\right)\frac{\left[-\left(\frac{\alpha_2}{\alpha}\right)J_0(\alpha_1 R_{1i}) + \left(\frac{\alpha}{\alpha_1}\right)(J_0(\alpha_1 R_{1e}) - J_0(\alpha_1 R_{1i}))\right]}{[Y_0(\alpha_1 R_{1i})J_0(\alpha_1 R_{1e}) - Y_0(\alpha_1 R_{1e})J_0(\alpha_1 R_{1i})]} \quad (22)$$

The physical unit of parameters K_{C1} and K_{D1} is given by the important factor $\sqrt{(\mu/(\sigma\omega))}$ that will be used afterwards. The factor (Z/Z_l) is just a correction factor that involves the correction length for the 2D geometry ($Z_l = Z + 2\Delta Z = Z(1+2\Delta Z/Z) \Rightarrow Z/Z_l = 1/(1+2\Delta Z/Z)$).

3.2.2. Inductor without field-shaper but tube

This case corresponds to case (b) of **Figure 4** and **Figure 5**. Two conducting regions are considered: the bulk 1-turn coil and the tube, separated by one air region: the airgap. Let's first define the skin depth δ_k (Eq. (23)) of regions $k=1$ (the tube), $k=3$ (the field-shaper) and $k=5$ (the coil) respectively

$$\delta_k = \frac{\sqrt{2}}{\alpha_k} = \sqrt{\frac{2}{\mu_k \sigma_k \omega}} \quad (23)$$

In addition to the limit condition and the constraint on H and j, we need to know the relationship between the secondary current I_1 in region 1 and the primary current $I_3=I$ in region 3. The induced voltage ratio is lower than 1 due to a flux ratio, which is weakened by the flux leakage in the airgap. This is as a result of the different crossed sections. Then the induced current ratio can be tuned by the different short-circuit resistances estimated by Lal and Hillier (1968). Let's assume a current transformation ratio β given by Eq. (24) and inspired from Lal and Hillier (1968) studies (the ideal transformation ratio is $m=1$).

$$\beta = \frac{-I_1}{I_3} = \frac{S_{\phi 1}}{S_{\phi 3}}\frac{R_3}{R_1} \approx \frac{\pi(R_{1e}-\delta_1)^2}{\pi(R_{3i}+\delta_3)^2}\frac{\delta_1 Z_1 (R_{3i}+\delta_3)}{(R_{1e}-\delta_1)\delta_3 Z}\frac{1}{m} \quad (24)$$

Then, the current conservation principle inside the coil section is given by Eq. (25) and the Maxwell-Ampere theorem applied onto the external limit of the coil section is given by Eq. (26):

$$I_3 = -\sigma_3 Z_3 i\omega \int_{R_{3i}}^{R_{3e}} A_3(r,\omega)dr \qquad (25)$$

$$I_3 - I_1 = \frac{Z_3}{\mu_3}\left(\frac{A_3(R_{3i},\omega)}{R_{3i}} + \partial_r A_3(R_{3i},\omega)\right) \qquad (26)$$

Likewise, the same physical principles inside the tube section and onto the external limit of the tube give equations (27) and (28):

$$-I_1 = -\sigma_1 Z_1 i\omega \int_{R_{1i}}^{R_{1e}} A_1(r,\omega)dr \qquad (27)$$

$$I_3 - I_1 = \frac{Z_1}{\mu_1}\left(\frac{A_1(R_{1e},\omega)}{R_{1e}} + \partial_r A_1(R_{1e},\omega)\right) \qquad (28)$$

We still assume a finite equivalent corrected inductor length Z_3 and tube length Z_1 along the z axis (most of the case $Z_3 \approx Z_1$).

3.2.3. Inductor with field-shaper and tube

This case corresponds to case (c) of **Figure 4** and **Figure 5**. Three conducting regions are considered: the bulk 1-turn coil, the field-shaper and the tube, separated by two air regions: the airgaps.

We still need to know the relationships between the secondary currents I_1 in region 1, I_3 in region 3, and the primary current I_5 in region 5. A slot is cut in the field-shaper, preventing any total current to cross its section. We can separate both sides of it, the one facing the tube crossed by the current I_3 and the one facing the coil crossed by the current ($-I_3$). Therefore, we propose two current transformation ratios β_{13} and β_{35} to be associated to airgaps 2 and 4 between regions 1 and 3 or 3 and 5 respectively.

$$\beta_{13} = \frac{-I_1}{I_3} = \frac{S_{\phi 1}}{S_{\phi 3}}\frac{R_3}{R_1} \approx \frac{\pi(R_{1e}-\delta_1)^2}{\pi(R_{3i}+\delta_3)^2}\frac{\delta_1 Z_1 (R_{3i}+\delta_3)}{(R_{1e}-\delta_1)\delta_3 Z_3}\frac{1}{m} \qquad (27)$$

$$\beta_{35} = \frac{-I_3}{I_5} = \frac{S_{\phi 3}}{S_{\phi 5}}\frac{R_5}{R_3} \approx \frac{\pi(R_{3e}-\delta_3)^2}{\pi(R_{5i}+\delta_5)^2}\frac{\delta_3 Z_3 (R_{5i}+\delta_5)}{(R_{3e}-\delta_3)\delta_5 Z}\frac{1}{m} \qquad (28)$$

Then, the current conservation inside the coil and the Maxwell-Ampere theorem applied around the coil give equations (29) and (30):

$$I_5 = -\sigma_5 Z_5 i\omega \int_{R_{5i}}^{R_{5e}} A_5(r,\omega)dr \qquad (29)$$

$$I_5 - I_3 = \frac{Z_5}{\mu_5}\left(\frac{A_5(R_{5i},\omega)}{R_{5i}} + \partial_r A_5(R_{5i},\omega)\right) \qquad (30)$$

In the following, we have to split the region 3 into two separated regions: the one facing region 5 (the coil), named region 35 (right side of field-shaper); and the one facing region 1 (the tube), named region 31 (left side of field-shaper). We then take the same physical principles inside sections of regions 35 and 31 (Eq. (31) & (32)) and onto the external limits of regions 35 and 31 (Eq. (33) & (34)).

$$-I_3 = -\sigma_3 Z_{35} i\omega \int_{R_{3e-10\delta_3}}^{R_{3e}} A_{35}(r,\omega)dr \qquad (31)$$

$$I_5 - I_3 = \frac{Z_{35}}{\mu_3}\left(\frac{A_{35}(R_{3e},\omega)}{R_{3e}} + \partial_r A_{35}(R_{3e},\omega)\right) \qquad (32)$$

$$I_3 = -\sigma_3 Z_{31} i\omega \int_{R_{3i}}^{R_{3i}+10\delta_3} A_{31}(r,\omega)dr \qquad (33)$$

$$I_3 - I_1 = \frac{Z_{31}}{\mu_3}\left(\frac{A_{31}(R_{3i},\omega)}{R_{3i}} + \partial_r A_{31}(R_{3i},\omega)\right) \qquad (34)$$

Finally, the same physical principles inside the tube section and onto the external limit of the tube give equations (35) and (36):

$$-I_1 = -\sigma_1 Z_1 i\omega \int_{R_{1i}}^{R_{1e}} A_1(r,\omega)dr \qquad (35)$$

$$I_3 - I_1 = \frac{Z_1}{\mu_1}\left(\frac{A_1(R_{1e},\omega)}{R_{1e}} + \partial_r A_1(R_{1e},\omega)\right) \qquad (36)$$

Each region has a finite corrected length Z_k along the z axis.

3.3. Alternative solution with the reduced magnetic vector potential A_i as a function of the voltage source ΔV

The solution of the equation (9) in the coil regions is found thanks to equation (12) and the coefficients variation principle. We thus look for the following solution given by Eq. (37):

$$A_i(r,\omega) = C(r)J_1(\alpha_1 r) + D(r)Y_1(\alpha_1 r) \qquad (37)$$

Introducing it inside Eq. (9), *C'(r)* and *D'(r)* must obey the following system:

$$\begin{Bmatrix} J_1(\alpha_1 r)\partial_r C + Y_1(\alpha_1 r)\partial_r D = 0 \\ \partial_r C \partial_r J_1(\alpha_1 r) + \partial_r D \partial_r Y_1(\alpha_1 r) = \frac{\mu\sigma\Delta V}{2\pi r} \end{Bmatrix} \quad (38)$$

Using the Wronskien, the solutions are:

$$C(r) = \left(C + \frac{\mu\sigma\Delta V}{4\alpha_1}\left(Y_0(\alpha_1 r) - Y_0(\alpha_1 R_i)\right)\right) \quad (39)$$

$$D(r) = \left(D - \frac{\mu\sigma\Delta V}{4\alpha_1}\left(J_0(\alpha_1 r) - J_0(\alpha_1 R_i)\right)\right) \quad (40)$$

where C and D are constants that can be determined by fixing the limit conditions (see next part). In the following, we will consider the whole regions, numbered from 0 to a maximum of 5. As a consequence, previous homogeneous Eq. (12) and non-homogeneous Eq. (37) solutions can be identified for each region with its number in index. Air regions cannot be avoided this time.

The solution to this problem can be found by computing a N*N matrix equation given in the Appendix B.2. for each of the following case (N=3, 8 or 15 depending on the number of regions; *i.e.* 2, 4 or 6 regions).

3.3.1. Inductor without field-shaper nor tube

This case corresponds to case (a) of **Figure 4** and **Figure 5**. 2 regions are considered: the coil (region 1) and the air (region 0).

We propose to use four limit conditions to determine the four coefficients C_0, D_0, C_1 and D_1: the value of the magnetic potential at $r=0$ equals 0 (Eq. (41)), the magnetic potential and the tangential component of the magnetic field H must be continuous at $r=R_{1i}$ (Eq. (42) and (43)), finally the circulation of the magnetic field H equals the current $I_1=I$ in the coil (*i.e.* the flux of the current density j) (Eq. (44)):

$$A_{i0} = 0 \Leftrightarrow D_0 = 0 \quad (41)$$

$$A_{i0}(R_{1i}, \omega) = A_{i1}(R_{1i}, \omega) \quad (42)$$

$$\frac{\left(\frac{A_{i0}(R_{1i})}{R_{1i}} + \partial_r A_{i0}(R_{1i})\right)}{\mu_0} = \frac{\left(\frac{A_{i1}(R_{1i})}{R_{1i}} + \partial_r A_{i1}(R_{1i})\right)}{\mu_1} \quad (43)$$

$$\frac{\left(\frac{A_{i1}(R_{1i})}{R_{1i}} + \partial_r A_{i1}(R_{1i})\right)}{\mu_1} = \int_{R_{1i}}^{R_{1e}} \left(-\frac{\sigma_1 \Delta V}{2\pi}\frac{Z}{Z_1} - i\sigma_1\omega A_{i1}\right) dr \quad (44)$$

3.3.2. Inductor without field-shaper but tube

This case corresponds to case (b) of **Figure 4** and **Figure 5**. Four regions are considered: the coil (region 3), the airgap between the coil and the tube (region 2), the tube (region 1) and the air region inside the tube (region 0).

We propose to use nine limit conditions to determine the eight coefficients C_0, D_0, C_1, D_1, C_2, D_2, C_3 and D_3 and the secondary current ($-I_1$) in region 1. Thanks to the reduced magnetic vector potential, we do not make any assumption (done with the total magnetic potential) on the magnitude and the phase shift of the current in the tube; the ones which were highlighted by Jablonski and Winkler (1978).

First the value of the magnetic potential at $r=0$ equals 0. The magnetic potential is continuous at $r=R_{1i}$, $r=R_{1e}$, $r=R_{3i}$. Then the tangential component of the magnetic field H must be continuous at $r=R_{1i}$, $r=R_{1e}$, $r=R_{3i}$. Finally, the circulation of the magnetic field H around the tube equals the current ($-I_1$) in the tube (Eq. (45)) and around the coil equals the current $I_3=I$ in the coil.

$$\frac{\left(\frac{A_{i1}(R_{1e})}{R_{1e}} + \partial_r A_{i1}(R_{1e})\right)}{\mu_1} - \frac{\left(\frac{A_{i1}(R_{1i})}{R_{1i}} + \partial_r A_{i1}(R_{1i})\right)}{\mu_1} = \frac{-I_1}{Z_1} \quad (45)$$

3.3.3. Inductor with field-shaper and tube

This case corresponds to case (c) of **Figure 4** and **Figure 5**. Six regions are considered: the coil (region 5), the airgap between the coil and the field-shaper (region 4), the field-shaper (3), the airgap between the field-shaper and the tube (region 2), the tube (region 1) and the air region inside the tube (region 0).

We propose to use sixteen limit conditions to determine the fourteen coefficients C_0, D_0, C_1, D_1, C_2, D_2, C_{31}, D_{31}, C_{35}, D_{35}, C_4, D_4, C_5 and D_5, the secondary current ($-I_1$) in region 1, and the intermediate current ($-I_3$) in region 3. In this case too, we do not make any assumption on the magnitude and the phase shift of the currents in the field-shaper and in the tube.

First the value of the magnetic potential at $r=0$ equals 0. Then this potential and the tangential component of H must be continuous at $r=R_{1i}$, R_{1e}, R_{3i}, R_{3e} and R_{5i}. Finally, the circulation of the field H around the tube equals the current ($-I_1$) in the tube, around the field-shaper equals zero ($-I_3+I_3$) (Eq. (46)) (which contains the 2 parts *31* and *35* of field-shaper) and around the coil equals the current $I_5=I$ in the coil.

$$\frac{\left(\frac{A_{i3}(R_{3e})}{R_{3e}}+\partial_r A_{i3}(R_{3e})\right)}{\mu_3} Z_5 - \frac{\left(\frac{A_{i3}(R_{3i})}{R_{3i}}+\partial_r A_{i3}(R_{3i})\right)}{\mu_3} Z_1 = 0 \qquad (46)$$

3.4. Derivation of local fields and densities

All the following physical quantities are derived from the unique magnetic vector potential in each region k. The magnetic flux density B, proportional to H, both in the z direction, is derived from either the total or reduced magnetic vector potential as follow:

$$B_k(r) = \mu_k H_k(r) = \left(\frac{A_k}{\mathrm{r}} + \partial_r A_k(\mathrm{r})\right) \qquad (47)$$

$$B_k(r) = \mu_k H_k(r) = \left(\frac{A_{ik}}{\mathrm{r}} + \partial_r A_{ik}(\mathrm{r})\right) \qquad (48)$$

The current density j, proportional to the electric field E, both in the θ direction, is also derived from the magnetic potentials as follow:

$$j_k(r) = \sigma_k E_k(r) = -i\sigma_k \omega A_k(r) \qquad (49)$$

$$j_k(r) = \sigma_k E_k(r) = -i\sigma_k \omega A_{ik}(r) - \frac{\sigma_k \Delta V}{2\pi r} \qquad (50)$$

The Lorentz force density f and the Maxwell stress tensor σ_b, both in the r direction, are finally derived as follow:

$$f_k(r) = real\left(j_k(r) B_k^*(r)\right) \qquad (51)$$

$$\sigma_{bk}(r) = -\frac{B_k(r) B_k^*(r)}{2\mu_k} \qquad (52)$$

3.5. Coils' parameters with approximation functions

In this section, we will focus on global coil parameters. First the definition of each parameter will be introduced, then the method to calculate these parameters will be explained. Finally, analytical formulae will be proposed thanks to exact values or good approximations of the base functions in the appendix. This might be very useful to make the sizing process and the feeding optimisation easier. The whole approximate analytical formulae, taking the frequency dependent skin depth into account, are given in the Appendix C.

3.5.1. Maximum induction and induction coefficient

The first performance criterion of a pulse inductor is the maximum magnitude of the induction $B_{k,max}$ generated in the airgap between the coil or the field-shaper numbered k ($k = 3$) and the tube. It is evident that $B_{k,max}$ is proportional to the current per unit length (I/Z). We thus suggest defining the maximum induction (Eq. (53)) and the induction coefficient (Eq. (54)) as follow.

$$B_{k,max} = max(|B_k|) \qquad (53)$$

$$K_b = \frac{B_{k,max}}{(I/Z)} \approx |K_{Ck}\alpha_{1k} J_0(\alpha_{1k} R_{ki}) + K_{Dk}\alpha_{1k} Y_0(\alpha_{1k} R_{ki})| \qquad (54)$$

The physical unit of K_b is given by μ_k.

3.5.2. Magnetic energy and equivalent inductance

Then we focus on the stored magnetic energy W_{mk} (Eq. (55)) of each region k and the equivalent inductance L (Eq. (56)), including the whole self and mutual inductances. Some authors proposed to calculate these inductances but never including eddy currents. Yu and Han (1987) calculated the quasi-static self-inductance of air core circular coils with a rectangular cross section. Conway (2007) gave the calculation for non-axial coils. Ravaud et al. (2010) added the calculation of the mutual inductance between two axial coils. Now, we propose to calculate the total inductance with the stored magnetic energy in the whole regions ($k = 0$ - 5), even in the presence of eddy currents. Due to the magnetic field damping in the skin depth of conducting regions, the inductance can be approximated by the one mainly due to the magnetic energy in air regions (k *even* $= 0, 2, 4$).

$$W_{mk} = 2\pi Z_k \int_{R_{ki}}^{R_{ke}} \frac{B_k B_k^*}{2\mu_k} r dr \qquad (55)$$

$$L = \frac{2W_m}{I^2} = \frac{2\sum_k W_{mk}}{I^2} = \sum_k L_k =$$

$$\sum_k \frac{\pi Z_k}{\mu_k Z^2} \int_{R_{ki}}^{R_{ke}} |K_{Ck}\alpha_{1k}J_0(\alpha_{1k}r) + K_{Dk}\alpha_{1k}Y_0(\alpha_{1k}r)|^2 r dr \approx$$

$$\sum_{k\ even} \frac{\pi \Delta R_k^2 Z_k}{\mu_k Z^2} |K_{Ck}\alpha_{1k}J_0(\alpha_{1k}R_{ke}) + K_{Dk}\alpha_{1k}Y_0(\alpha_{1k}R_{ke})|^2 \quad (56)$$

The physical unit of L is given by $(\pi \Delta R_k^2/Z_k)\mu_k$.

3.5.3. Joule losses and equivalent resistance

$$P_{jk} = 2\pi Z_k \int_{R_{ki}}^{R_{ke}} \frac{j_k j_k^*}{2\sigma_k} r dr \quad (57)$$

$$R = \frac{2P_j}{I^2} = \frac{2\sum_k P_{jk}}{I^2} = \sum_k R_k \approx$$

$$\sum_{k\ odd} \frac{\pi \sigma_k \omega^2 Z_k}{Z^2} \int_{R_{ki}}^{R_{ke}} |K_{Ck}J_1(\alpha_{1k}r) + K_{Dk}Y_1(\alpha_{1k}r)|^2 r dr \quad (58)$$

Then we focus on the Joule power losses P_{jk} (Eq. (57)) of each region k (k *odd = 1, 3, 5*) and the equivalent resistance R (Eq. (58)), including the resistance R_k of each region k. The physical unit of R is given by $(\sigma_k Z_k)^{-1}$.

3.5.4. Lorentz force and force coefficients

Now we focus on the surface maximum Lorentz force density F_k (Eq. (59)) and the global magnetic pressure (*i.e.* the integrated Lorentz force density) responsible for the deformation Pf_k (Eq. (61)), at the surface and inside the volume of each region k. We show that both depend on the product between the squared current per unit length $(I/Z)^2$ and the square root of the angle velocity $\sqrt{\omega}$. This leads us to define the following corresponding force coefficients:

$$F_k = max(|f_k(r)|) = |f_k(R_{ki})| \ or \ |f_k(R_{ke})| \quad (59);\ K_{fk} = \frac{F_k}{\sqrt{\omega}\left(\frac{I}{Z}\right)^2} \quad (60)$$

$$P_{fk} = \int_{R_{ki}}^{R_{ke}} f_k(r) dr \quad (61);\ K_{ik} = \frac{|P_{fk}|}{\sqrt{\omega}\left(\frac{I}{Z}\right)^2} \quad (62)$$

The physical units of F_k (Eq. (59)) and Pf_k (Eq. (61)) are given by $(\mu_k/\delta_k)(I/Z)^2$ and $(\mu_k \Delta R_k/\delta_k)(I/Z)^2$ respectively. The physical units of K_{fk} (Eq. (60)) and K_{ik} (Eq. (62)) are given by $(\sigma_k^{1/2}\mu_k^{3/2})$ and $(\sigma_k^{1/2}\mu_k^{3/2}\Delta R_k)$ respectively.

3.5.5. Maxwell stress tensor and coefficients

Finally, we study the maximum magnitude of the Maxwell stress tensor along the radius P_{sk} (Eq. (63)) at the surface of each region k. This depends on the squared current per unit length $(I/Z)^2$. This leads to the corresponding and following stress coefficient (Eq. (64)):

$$P_{sk} = max(|\sigma_{bk}(r)|) = |\sigma_{bk}(R_{ki})| \ or \ |\sigma_{bk}(R_{ke})| \quad (63)$$

$$K_{sk} = \frac{P_{sk}}{\left(I/Z\right)^2} \approx \frac{|K_{Ck}\alpha_{1k}J_0(\alpha_{1k}R_{ki}) + K_{Dk}\alpha_{1k}Y_0(\alpha_{1k}R_{ki})|^2}{\mu_k} \quad (64)$$

The physical units of Pf_k are given by $\mu_k(I/Z)^2$. The physical units of K_{sk} are given by μ_k.

3.6. Simulation results without field-shaper

In this section, we compare the main calculation results to both 2D and 3D numerical simulations performed with the Finite Element Method. The first test case (*TESTCASE 1*) studied contains a 1-turn massive coil with or without a tube but no field-shaper. The value of the input variables such as the geometry and the material properties are given in the Appendix D.1.

First, 2D and 3D models take more time to compute (1 hour and 1 week minimum respectively) than the 1D models (1 minute at maximum). The results in **Table 1** give similar values. In 3D the terminals, connectors and the base can be modeled. 2D and 3D calculations of the impedance (R, L) and the voltage (ΔV) give closer values (<15%) when we limit the calculation inside the ring part of the coil in 2D and in 3D, results show higher discrepancies (>15%) when adding the base, the terminals and the connectors only in 3D (this is not possible in 2D). The maximum force density has been compared on the $\Delta_{3D(\theta=90°)}$ and Δ2D axis respectively (see **Figure 2**). Only 15 % discrepancies were noticed comparing 2D and 3D results for different axis ($\Delta_{3D(\theta=180°)}$). These inaccuracies might mainly due to the θ dependences and the slot and would require a complete 3D analysis.

3.6.1. Fields and densities with and without a tube

Providing the current I (with the total magnetic potential A model) or the voltage ΔV (with the reduced magnetic potential A_i model) and the angle velocity ω or the frequency f; the magnetic field, current density and force density can be computed (see **Figure 6**).

Table 1: Current (kA), voltage (V) and maximum force density ($GN.m^{-3}$) results without field-shaper (*TESTCASE 1*).

	1D (A)	1D (A_i)	2D	3D
$\Delta V_{without\ tube}$	**$2494e^{i1.5}$**	**2800**	**$2705e^{i1.5}$**	**$2778e^{i1.5}$**
$I_{3,\ without\ tube}$	**825**	**$813e^{-i1.5}$**	**825**	**825**
$\Delta V_{with\ tube}$	**$797e^{i1.12}$**	**800**	**$970e^{i1.17}$**	**$1287e^{i1.28}$**
$I_{3,\ with\ tube}$	**825**	**$795e^{-i1.14}$**	**825**	**825**
$I_{1,\ with\ tube}$	**$696e^{-i3.13}$**	**$633e^{-i0.98}$**	**$710e^{-i3.1}$**	**$678e^{-i3.1}$**
$F_{1,\ with\ tube}$	**1187**	**978**	**1116**	**965**

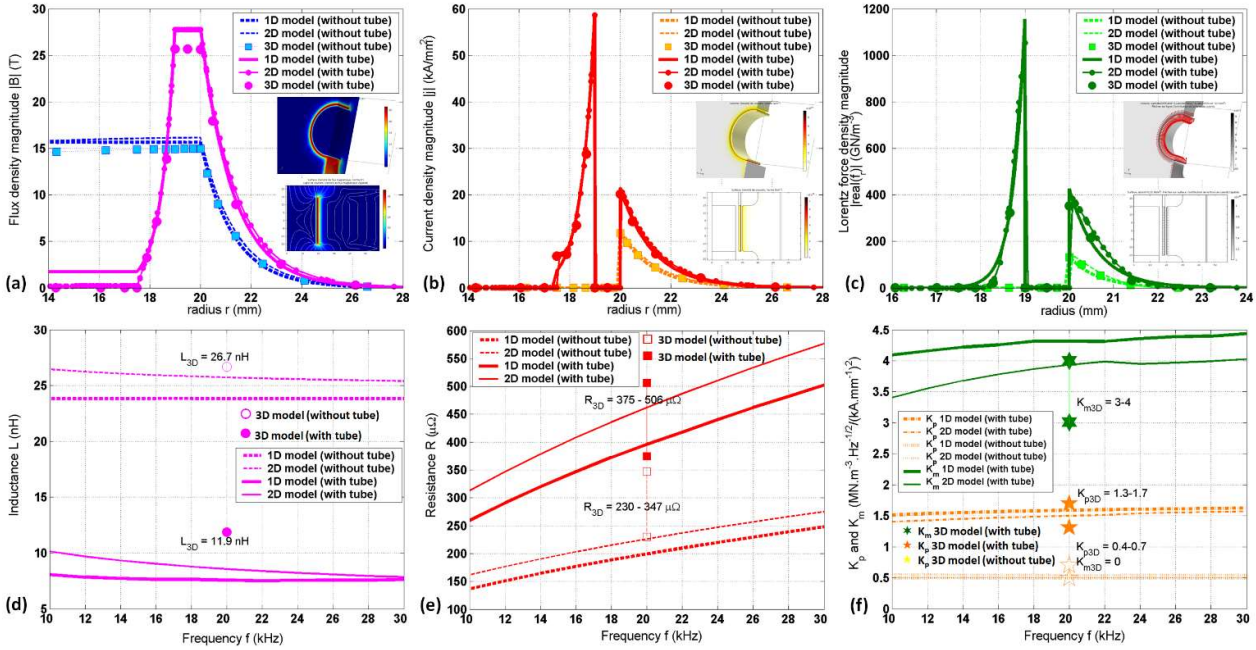

Figure 6. (top) Radial distribution of magnetic flux density B (a), current density j (b) and Lorentz force density f_r. (c) (bottom) Inductance L (d) resistance R (e) and maximum force density coefficients K_p and K_m (f) *($\Delta Z \approx 16.5$ mm) (TESTCASE 1)*. Worse discrepancies stay below 25% and best ones stay below 5%.

Curves (a), (b) and (c) of **Figure 6** are important to check the coherence in qualitative shape and skin depth of calculated field B and densities j and f_r distributions with different models. The coil generates a magnetic flux in the air with a quasi-constant induction while it exponentially decreases in the coils' skin depth ($3\delta_3 = 4.5$ *mm*). The tube acts as a screen for this flux such that it stops and is created only in the air gap between the coil and the tube. Therefore, the flux density also rapidly decreases in the tube's skin depth ($3\delta_1 = 1.59$ *mm*). Both skin effects are due to eddy currents in the conducting regions, induced by the flux variations. This leads to a total current density located mainly at the internal surface of the coil and the external surface of the tube.

3.6.2. Frequency dependent coils' parameters

Curves (d), (e) and (f) of **Figure 6** and **Table 2** give the main coil parameters, computed either with the 3D, the 2D or the 1D model. The inductance comes from the magnetic energy in air (mainly dependent on the geometry no matter what frequency) and a small amount of energy in the skin depth of conducting regions (the latter depending on the frequency). The higher the frequency, the lower the coils surface and the inductance. The tube is behaving like a secondary coil in short circuit with a mutual inductance that has to be subtracted

from the self-inductance. As a result, the total equivalent inductance L with a tube is lower. The resistance comes from the Joule losses with dependence on the coil circumference and skin depth (so frequency dependent). The higher the frequency the smaller the skin depth and the conductance $G=1/R$. The tube, as another conducting region, introduces an additional resistance. As a result, the total resistance R with a tube is higher. Adding the resistance of the terminals will also result in a higher total resistance. R value given in 3D is the mean value of the ring part of the coil (see large range of 3D values in **Figure 6** (e) and (f)). The limiting error is only acceptable for L, K_p and K_m. The latter seem to be more influenced by what happens in the turning parts around the tube than determined by the coils ends. Fortunately, the voltage and the force are much more dependent on the inductive part (from 80 to 98% of the voltage) rather than the resistive part (from 2 to 20% of the voltage). The maximum induction coefficient (maximum induction, created by the coil in the useful airgap near the tube, per Ampere per unit length) is higher with a tube due to field sources in two regions instead of one.

Table 2: Equivalent resistance R ($\mu\Omega$), inductance L (nH), maximum induction coefficient K_b ($T/(kA/mm)$) and maximum force coefficients K_p in the coil and K_m in the tube ($MN.m^{-3}.s^{1/2}/(kA/mm)^2$) results without and with tube (@ *20 kHz*) for *TESTCASE 1*.

	Without tube			With tube		
	1D	2D	3D	1D	2D	3D
R	**200**	**226**	**290**	**400**	**462**	**446**
L	**24**	**27**	**26.7**	**7**	**8.6**	**11.9**
K_b	**0.6**	**0.59**	**0.54**	**1**	**1.01**	**0.93**
K_p	**0.63**	**0.55**	**0.50**	**1.77**	**1.5**	**1.31**
K_m				**4.25**	**4.0**	**3.5**

3.6.3. Air-Gap Sensitivity analysis

The major advantage of reduced analytical models is to speed the calculations especially in a sensitivity analysis when varying several parameters. For the couplings of electromagnetic, electrical and mechanical parts the most critical parameter we must take into account is the air gap g between the coil and the tube. It is very important to correctly estimate the varying resistance $R(g)$, inductance $L(g)$ and force coefficient $K_m(g)$. We can save time by relying on 2D FEM simulations, that has been previously validated thanks to a 3D FEM simulation. As shown in **Figure 7**, the typical values and tendencies of $R(g)$, $L(g)$ and $K_m(g)$ as a function of the increasing air gap g are described with both the 2D and 1D models and are coherent with each other. Because the distance between the two parts becomes bigger, interactions and eddy currents inside the tube become weaker. It is logical to see that both the resistance R and the force coefficient K_m decrease as a function of g. Meanwhile, because the negative mutual effect is also weakened, the equivalent inductance L will increase as a function of g. The first derivative $\partial_g L$ of this last function will play an important role.

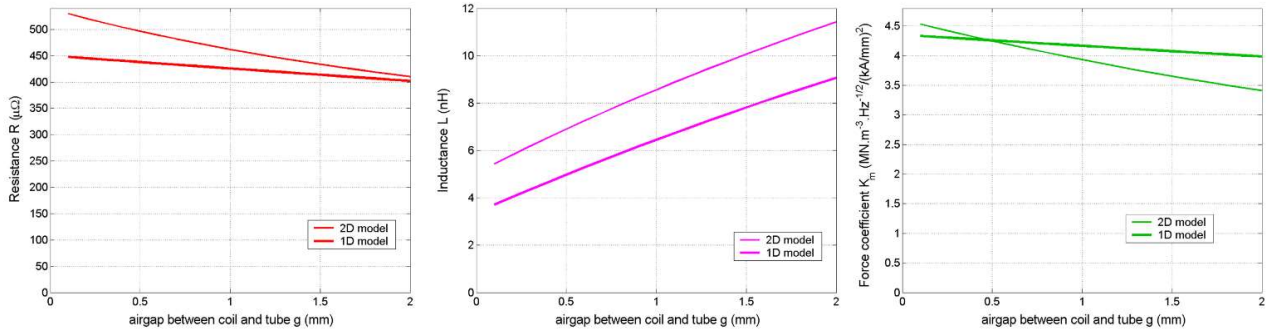

Figure 7. Variation of resistance R, inductance L and force coefficient K_m as a function of the airgap g between coil and tube (*TESTCASE 1*).

3.7. Simulation results with field-shaper

The second test case (*TESTCASE 2*) studied contains a 1-turn massive coil and a field-shaper with or without a tube. The value of the input variables such as the geometry and the material properties are given in the Appendix D.2. Results of **Table 3** are close and coherent. The 3D computation with field-shaper does not provide fast enough as good of result as 2D or 3D computations without field-shaper. This is mainly due to the tremendous number of nodes required to get a mesh fine enough in the four very thin cylindrical parts. That's also why we investigate an analytical model which will give accurate enough results much faster and less time and memory consuming.

Table 3: Current (kA), voltage (V) and maximum force density ($GN.m^{-3}$) results with field-shaper (*TESTCASE 2*)

	1D (A)	1D (A_i)	2D
$\Delta V_{without\ tube}$	**$4153e^{i1.4}$**	**3600**	**$3780e^{i1.4}$**
$I_{5,\ without\ tube}$	**825**	**$840e^{-i1.33}$**	**825**
$\Delta V_{with\ tube}$	**$1670e^{i1.15}$**	**2500**	**$1962e^{i1.13}$**
$I_{5,\ with\ tube}$	**825**	**$770e^{-i1.04}$**	**825**
$I_{1,\ with\ tube}$	**$648e^{-i3.13}$**	**$603e^{-i1.22}$**	**$670e^{-i3.1}$**
$F_{1,\ with\ tube}$	**944**	**880**	**967**

3.7.1. Fields and densities without and with tube

Providing the current I (or the voltage ΔV) and the angle velocity ω, the induction B, current density j and force density f_r are computed (focus on the second airgap between the field-shaper and the tube, curves (a), (b) and (c) of **Figure 8**). The field-shaper is acting as a secondary coil that stops the induction and concentrates it in the first air gap between the coil and the field-shaper; but re-submit the tube to the flux imposed by the coil. Therefore, the flux density is also rapidly decreasing inside the field-shaper's skin depth ($3\delta_3 = 2\ mm$).

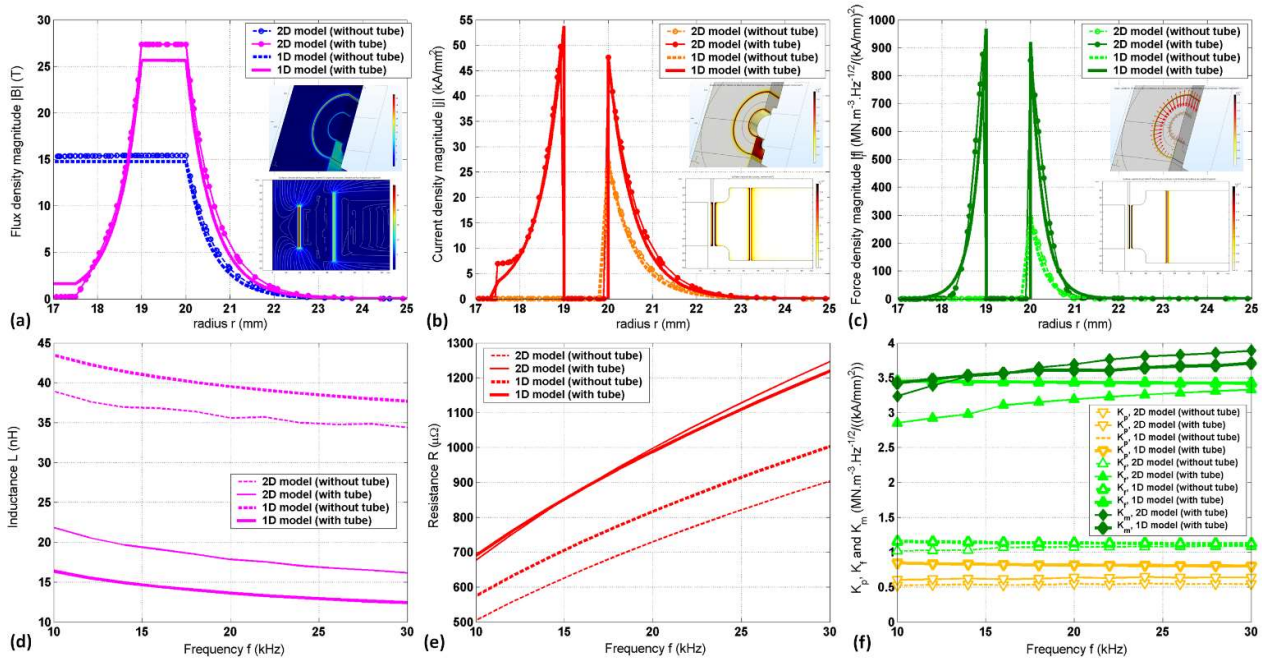

Figure 8. (top) Radial distribution of magnetic flux density B (a), current density j (b) and Lorentz force density f_r. (c) (bottom) Equivalent inductance L (d), resistance R (e) and maximum force density coefficients K_p, K_f and K_m (f) *($\Delta Z \approx 16.5\ mm$) (TESTCASE 2).*

3.7.2. Frequency dependent coils' parameters

Curves (d), (e) and (f) of **Figure 8** and **Table 4** give the coil parameters, computed with either the 2D or the 1D model. The dependencies of the parameters on the frequency are unchanged due to the same physical phenomenon as stated previously: the frequency dependent skin effect. The field-shaper, as a third conducting region, introduces an additional resistance. To form the same tube, due to a

bigger coils' section, the inductance L is also bigger with a field-shaper than without. The mutual force coefficient K_m is weakened by the two airgaps using a field-shaper, which is only useful to adapt the radius of a given coil to form a tube with a different lower radius.

Table 4: Equivalent resistance ($\mu\Omega$), inductance (nH), maximum induction coefficient K_b ($T/(kA/mm)$) and maximum force coefficients K_p in the coil, K_f in the field-shaper and K_m in the tube ($MN.m^{-3}.s^{1/2}/(kA/mm)^2$) results without and with tube (@ *20 kHz*) for *TESTCASE 2*.

	Without tube		With tube	
	1D	2D	1D	2D
R	**820**	**730**	**998**	**1000**
L	**39**	**36**	**14**	**17.2**
K_b	**0.54**	**0.56**	**0.93**	**0.99**
K_p	**0.65**	**0.5**	**0.8**	**0.64**
K_f	**1.13**	**1.07**	**3.5**	**3.2**
K_m			**3.6**	**3.7**

4. Transient coupling considerations and comparisons

As shown previously, the main parameters of the coil depend on the natural frequency f_n of the current pulse and of the changeable air-gap $g=g_2$ between the coil and the tube (*i.e.* linked to the deformation). We also show that $\omega_n=2\pi f_n$ depends on the coil parameters, and so on the deformation too. As a consequence, electrical, mechanical and electromagnetic phenomena should be coupled as follow.

4.1. Equivalent electrical circuit coupling

The coil with or without a field-shaper, and with or without tube is considered as an inductor with an equivalent inductance $L(g,\omega)$, an equivalent electrical resistance $R(g,\omega)$ and an equivalent mechanical resistance $R_m(g,g',\omega)$ when the tube is deformed. A simple equivalent electrical circuit is proposed in **Figure 9**. Once the capacitor C of the generator is charged at a given voltage V_0, a switch is closed to let a current pulse circulate in cables of equivalent resistance R_1 and inductance L_1 towards the inductor.

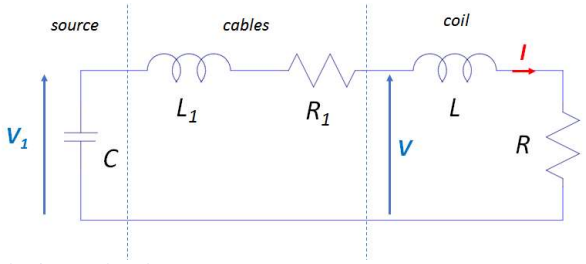

Figure 9. Equivalent electrical circuit of magnetic pulse system.

Considering first a constant position of the tube without deformation ($g'=0$), the natural angle velocity $\omega_n=2\pi f_n$ and the phase angle β between the current I and the voltage V_1 pulses must obey the following equations proposed by Otin et al. (2011) (65):

$$\omega_n = \sqrt{\omega_0^2 - \left(\frac{1}{\tau}\right)^2} \text{ and } \beta = \tan^{-1}(\tau\omega_n) \qquad (65)$$

with $\omega_0 = 1/\sqrt{C(L_1+L)}$ and $\tau = \big(2(L_1+L)\big)/(R_1+R)$

Once the natural oscillating frequency is determined, it is then possible to deduce the equivalent electrical components of the coil (with or without the field-shaper or/and the tube). The inductance L and the resistance R are given in equations (56) and (58). The equivalent mechanical resistance R_m, which is also proposed by Lal and Hillier (1968), can be deduced from $L(g)$ by the following relationship (66):

$$R_m = \left(\frac{\partial L}{\partial g}\right)\left(\frac{\partial g}{\partial t}\right) = (\partial_g L)(\partial_t g) = (\partial_g L)g' \qquad (66)$$

Given the initial conditions on the voltage and the current ($\Delta V(t=0) = V_0$, $I(t=0) = 0$), it is then possible to calculate the voltage and current pulses from time to time with the help of the following ordinary differential equations (67):

$$\left\{\begin{array}{c} V_1 = (R_1 + R_m + R)I + (L_1 + L)\frac{\partial I}{\partial t} \\ I = C\frac{\partial V_1}{\partial t} \end{array}\right\} \quad (67)$$

The natural frequency and the equivalent components R, L and R_m can change from time to time if the airgap g change.

4.2. Mechanical coupling solution(s)

The maximum force induced by the current pulse inside the coil and the tube can be estimated thanks to equation (59) by its transient expression Eq. (68). The global magnetic pressure responsible for the deformation Eq. (61) is equivalently given by Eq. (69).

Due to the shape of the pseudo-harmonic solution and the square root of ω; both the force and the strength can be derived from the squared current $I(t)/Z$ per unit length thanks to the fractional derivative operator $\partial(.)/\partial t^{1/2}$. $\Gamma(x)$ is the gamma function defined by an extension of the factorial function with its argument shifted down by 1: $\Gamma(x)=(x-1)!=\int_{u>0}(u^{x-1}e^{-u})du$

$$F_k = \frac{K_{fk}}{2}\frac{\partial\left(\left(I/Z\right)^2\right)}{\partial t^{1/2}} = \frac{K_{fk}}{2}\sqrt{\frac{\pi}{4}}\frac{\Gamma(3)}{\Gamma\left(\frac{5}{2}\right)}\frac{\partial\left(I/Z\right)}{\partial t^{1/2}}\left(I/Z\right)^{3/2} \quad (68)$$

$$P_{fk} = \frac{K_{ik}}{2}\frac{\partial\left(\left(I/Z\right)^2\right)}{\partial t^{1/2}} = \frac{K_{ik}}{2}\sqrt{\frac{\pi}{4}}\frac{\Gamma(3)}{\Gamma\left(\frac{5}{2}\right)}\frac{\partial\left(I/Z\right)}{\partial t^{1/2}}\left(I/Z\right)^{3/2} \quad (69)$$

The magnetic pressure $P_{fk}(t)$ is counterbalanced by the mechanical stress $s(t)$, which depends on the mechanical deformation $\varepsilon(t)$ and the deformation speed $\varepsilon'(t)$ as follows Eq. (70). The law of Johnson and Cook (1983), whose relevance has been demonstrated by (Shang et al., 2012), is proposed for high speed forming processes but still neglecting the visco-plastic energy dissipation.

$$s = min\left(E\varepsilon, (S_1 + S_2\varepsilon^n)\left(1 + S_3\ln\frac{\varepsilon'}{\varepsilon_0'}\right)\right) \quad (70)$$

Where E is the Young modulus. S_1, S_2, S_3, n and ε_0' are mechanical properties of the material (see Appendix E.). When considering the field-shaper and the coil, only the young modulus and elastic deformations are taken into account.

Then the material will deform itself following the physical dynamical Eq. (71) inspired from various authors. Jablonski and Winkler (1978) included a similar mechanical equation while analysing the electromagnetic forming process. Daehn et al. (2008) used an analogous law but for magnetic pulse welding of sheet connections. Hahn et al. (2016) had to consider the same dynamical equation when interpreting experiments with simulations. The proposed 1D Eq. (71) gives the acceleration g'' of airgap g time variations.

$$g'' = \frac{1}{\gamma_k(R_{ke}-R_{ki})}\left(P_{fk} - s_k\ln\frac{R_{ke}}{R_{ki}}\right) \quad (71)$$

Where s_k is the mechanical stress, γ_k is the volume mass density of the material and $e_k=(R_{ke}-R_{ki})$ is the thickness, of region k (tube, field-shaper or coil depending on the case). Eq. (71) is usable only for the forming and crimping processes. The welding process conditioned by an impact angle and analysed by Raoelison et al. (2012) cannot be simplified by an equivalent 1D problem like for the forming and crimping process, it requires a 2D model with the two variables (r,z).

4.3. Flow-chart of the coupling solution

Each modelling tool has been previously defined (the mechanical model, the electrical model, the natural resonant frequency model and the electromagnetic model). The coupling procedure is shown on the flow chart of **Figure 10**. It is then possible to carry out the transient calculation of the voltage, the current, the force, the deformation and the speed of deformation.

4.4. Simulations Results

The aim of the 1D model is to estimate with accuracy the forces induced inside the coil and the tube and the current pulse needed. The force in the coil is the main cause of the self-damaging process. The force in the tube is useful for the forming process. The energy of the first pulse is important in the process and it is described by the 1D model that gives results close to the 2D one (see **Figure 11**).

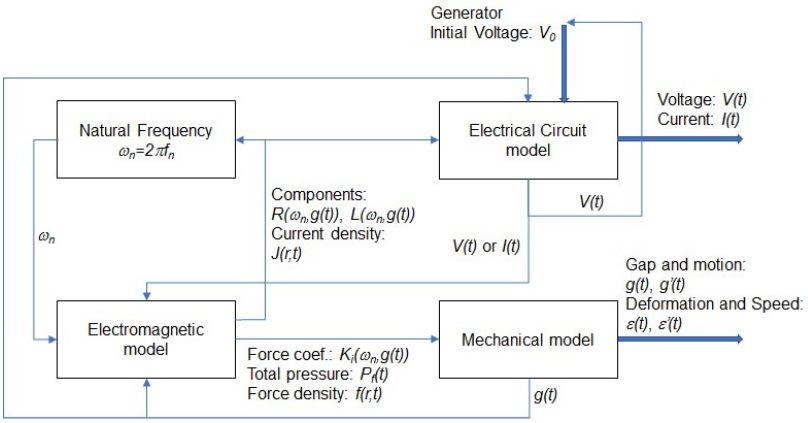

Figure 10. Flow-chart of the coupling solution with electromagnetic, electrical and mechanical problems.

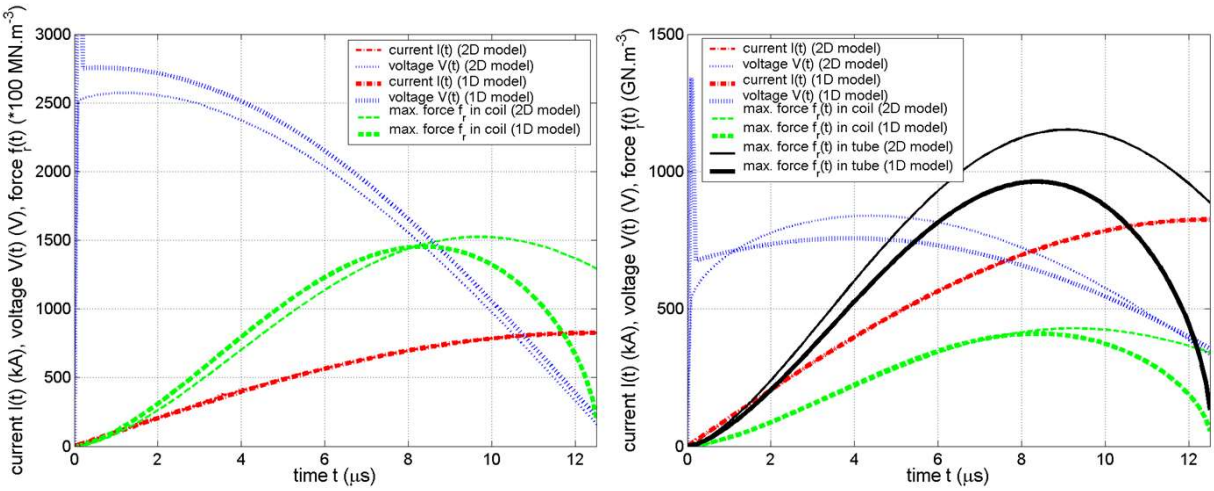

Figure 11. (a. LEFT) Current, voltage and maximum force simulation as a function of time for the coil without field-shaper nor tube (*TESTCASE 1*). (b. RIGHT) Current, voltage and maximum force simulation as a function of time for the coil without field-shaper but tube (*TESTCASE 1*).

5. Experimental and numerical results

Experiments measurements have been carried out on two inductors, dedicated to industrial applications. The first prototype (*TESTCASE 3*) is a 1-turn massive or bulk coil made of steel without field-shaper (see the Appendix E.1, with normalized data due to a non-disclosure agreement). The second prototype (*TESTCASE 4*) is a 1-turn massive or bulk coil with a field-shaper, both made of copper alloys materials partly studied by some authors. Arnaud et al. (1985) studied the electrical and mechanical properties of copper alloys. Lockyer and Noble (1999) proposed some fatigue mechanisms inside similar copper alloys (CuNiSi). Two new materials named the Siclanic® and Cuprofor® materials (@ Le Bronze Alloys) have been used in the present paper with a known electrical conductivity but no complete characterisations yet (description is in the Appendix E.2.).

5.1. TESTCASE 3: coil without field-shaper

5.1.1. Coils electrical parameters

The first step is to compute L and R with or without the tube as a function of the frequency and the air gap. Results on *TESTCASE 3* are given in **Figure 13**. The two models are in agreement with each other. The resulting current-voltage characteristics which are computed in the transient working condition with respect to the equivalent components of **Figure 13** also fit the measurements (see **Figure 12**). We can obtain an approximate for the current and voltages pulses measured from the equations of Eq. (72).

$$\begin{cases} V_1(t) = V_0\omega_0\omega_n^{-1}\, exp(-t/\tau)sin(2\pi f_n t+\beta) \\ V(t) = \sqrt{(R-L/\tau)^2+(L\omega_n)^2}\, I_p\, exp(-t/\tau)sin(2\pi f_n t+\gamma) \\ I(t) = I_p\, exp(-t/\tau)sin(2\pi f_n t) \end{cases} \quad (72)$$

$I_p \propto V_0 C \omega_0^2 \omega_n^{-1}$ is the current peak parameter (dependent on the initial voltage V_0, C, f_0 and f_n), $\gamma = tan^{-1}((L\omega_n)/(R-L/\tau))$ is the phase angle between I and V, τ is the time decay constant and f_n is the natural frequency. Finally, it has to be mentioned that despite the usual magnetic properties of steel, high energy measurements with enormous peak currents will induce a magnetic saturation. As a result, the steel is considered as a non-magnetic material ($\mu = \mu_0$) like most of the conducting materials usually used for this purpose.

5.1.2. Transient electrical behaviour

In **Figure 12**, the total transient current I is enforced. It is given by Eq. (72) with a current peak parameter I_p=*175.6 kA* (with tube) and *165.7 kA* (without tube), a time constant τ=*41.7 µs* (with tube) and *43.5 µs* (without tube), with no phase angle and a natural frequency f_q = *27.5 kHz* (with tube) and *27 kHz* (without tube).

The current and voltages have been measured (**Figure 12**). The model allows the computation of the pulses with a good accuracy except for the smaller voltage V with the tube (see next and **Figure 14** for improvements), but neglects higher frequencies mainly due to the spark gaps between the generator and the inductor.

5.1.3. Transient local force without deformation

In **Figure 13**, the total transient current I is given by Eq. (72) with a peak current I_p = *774 kA*, a time constant τ = *50 µs*, with no phase angle and a natural frequency f_q = *22 kHz* (with tube, σ_1 = *30 % IACS*). We compare the force density at time steps *7 µs* and *10 µs* and estimate the discrepancies between the 2D (axis Δ_{2D}) and the 3D model (average of axis $\Delta_{3D(\theta=90°)}$ and $\Delta_{3D(\theta=180°)}$) to be below 10%.

5.2. TESTCASE 4: coil with field-shaper

The second test case (*TESTCASE 4*) measured contains a 1-turn massive coil and a field-shaper with or without a tube. The confidential variables such as the geometry and the material properties are defined and normalised in the Appendix E.2.

5.2.1. Coil parameters

Table 5 Gives the experimental identification and calculation of parameters R and L. We observe important inaccuracies especially in case (**b**) (coil + field-shaper). The measurement data contains lots of dispersion (from 20 to 40 % for L and 30 to 60 % for R). Case (**a**) (coil) and (**c**) (coil + field-shaper + tube) are however correctly described with coherent values inside the dispersion range.

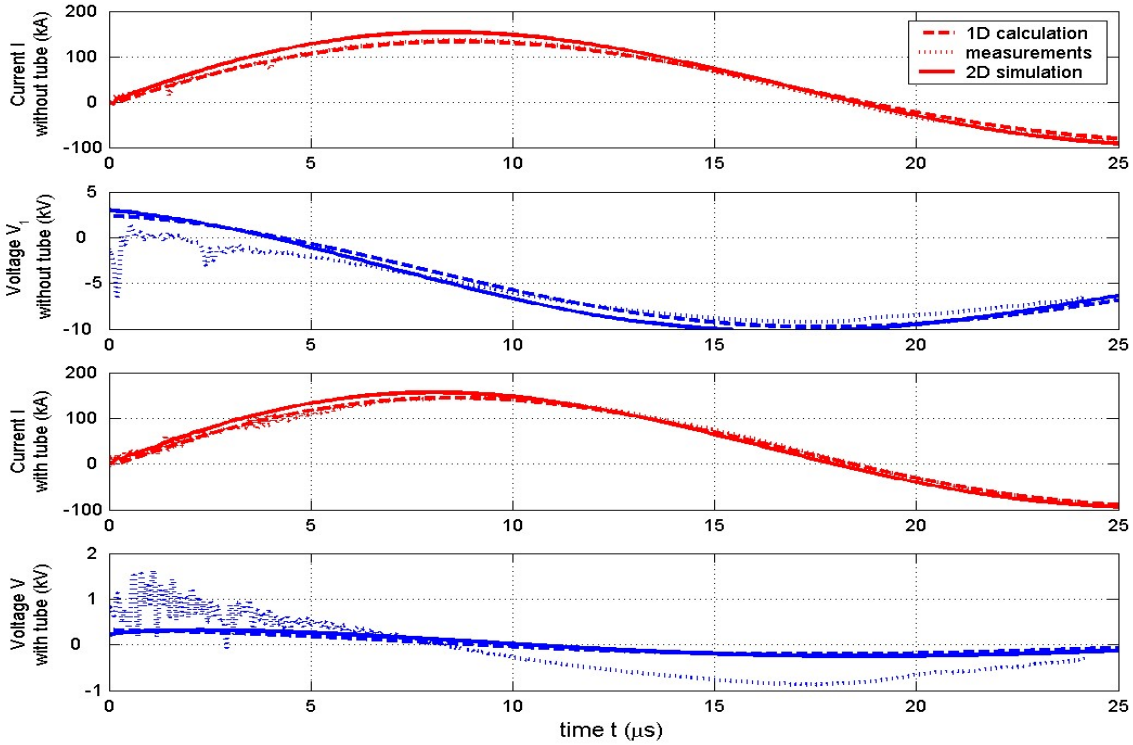

Figure 12. Transient current I and voltage V_1 or V pulses as a function of time with and without tube for the *TESTCASE 3* @ BASIS EP.

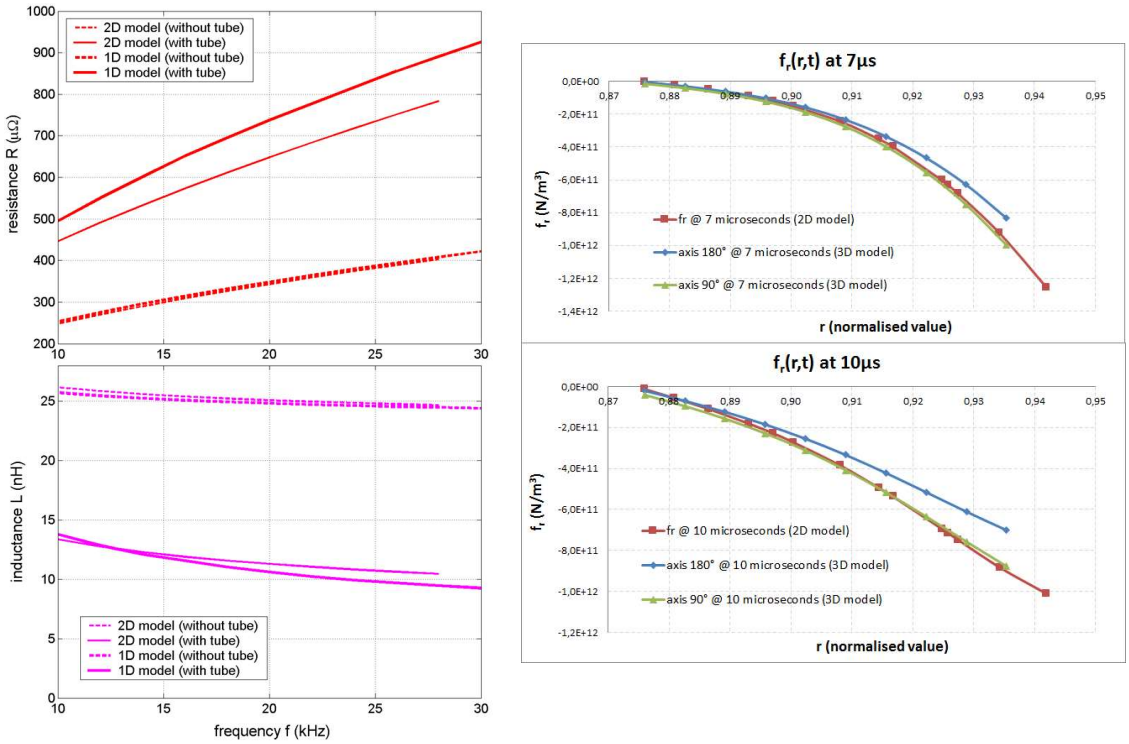

Figure 13. (LEFT) Calculation of equivalent resistance and inductance for *TESTCASE 3*. Comparison between 1D and 2D models (*ΔZ ≈ 12.5 mm)*)) (RIGHT) Calculation of transient local Lorentz force density as a function of normalised radius in tube at various time step. Comparison between 2D models (@ESIEE) and 3D model (@UTC) for *TESTCASE 3*.

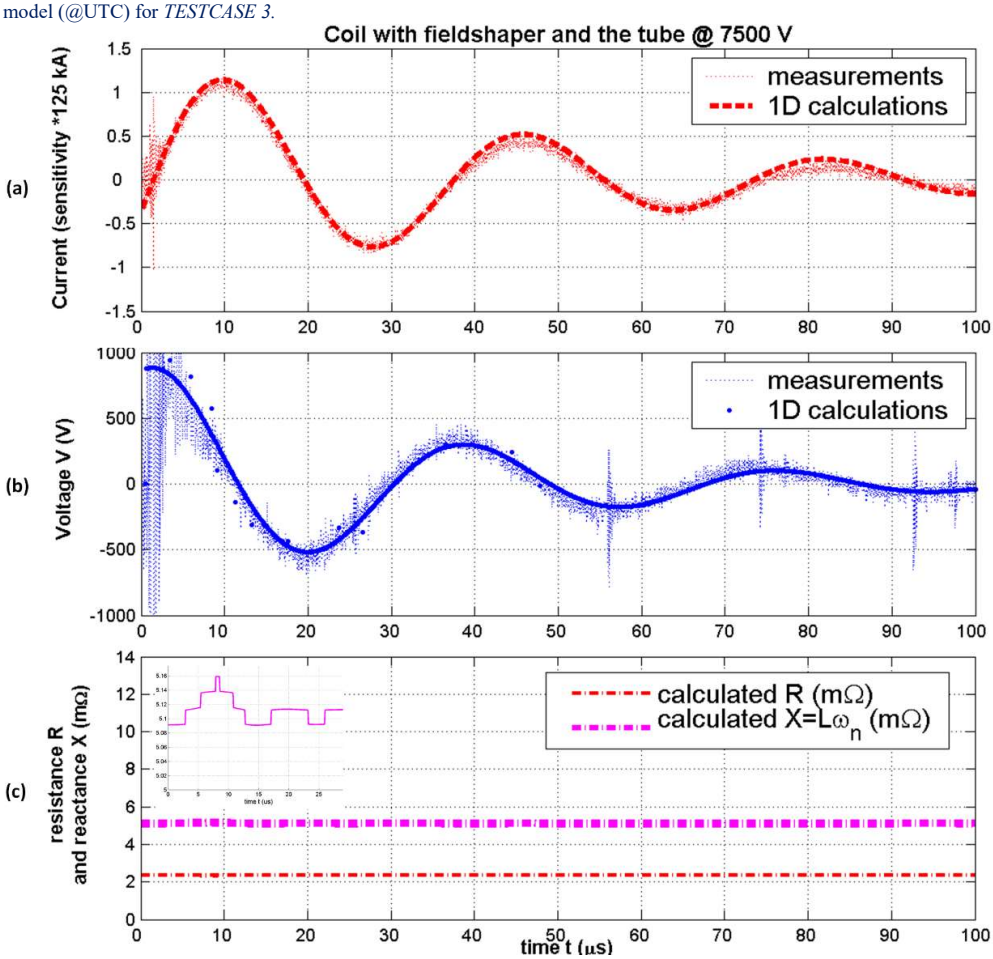

Figure 14. 1D calc. & meas. of the current (**a**), the voltage (**b**) and the impedance (**c**), with field-shaper & tube *@ V_0 = 7500 V* (*ΔZ ≈ 4 mm*) (*TESTCASE 4*).

Table 5: Electrical parameters calculation and identification of *TESTCASE 4*.

case	Method	*R (μΩ)*	*L (nH)*	*f(kHz)*	*τ (μs)*
(a)	*Model*	**203**	**84**	**24.4**	**49.8**
coil	*Meas.*	**200 - 380**	**75 ± 15**	**24.8 ± 0.3**	**48.9 ± 4**
(b)	*Model*	**1840**	**53**	**25.6**	**39.5**
coil+field-shaper	*Meas.*	**45 - 1545**	**50 ± 13**	**25.8 ± 0.4**	**42.2 ± 5**
(c)	*Model*	**2400**	**29**	**26.8**	**34.5**
coil+field-shaper+tube	*Meas.*	**1 - 2440**	**25 ± 10**	**27.2 ± 0.6**	**38.5 ± 7**

Results have been identified with equations (73) and (74), or calculated with equations (58) and (56).

$$R = \frac{(2/\tau)}{C\left((2\pi f)^2 + (1/\tau)^2\right)} - R_1 \qquad (73) \text{ and } L = \frac{1}{C\left((2\pi f)^2 + (1/\tau)^2\right)} - L_1 \qquad (74)$$

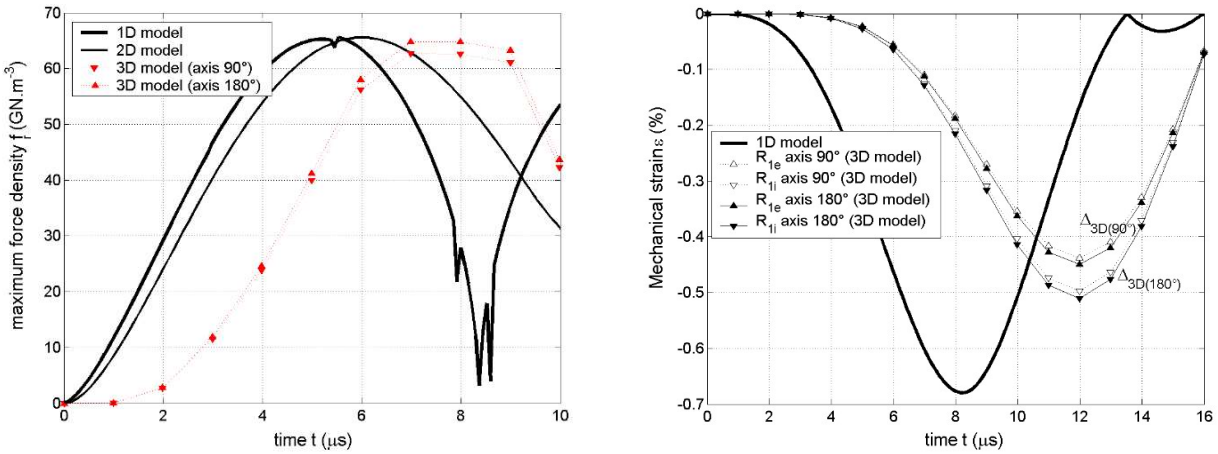

Figure 15. (a. LEFT) Absolute surface and maximum force density (*TESTCASE 4*). Comparison between 1D, 2D and 3D models (LS Dyna) (@PFT Innovaltech). (b. RIGHT) Transient elastic strain or deformation (*TESTCASE 4*). Comparison between 1D and 3D models (LS Dyna) (@PFT Innovaltech)

5.2.2. Results without plastic deformation

Figure 14 shows the current-voltage characteristics of the coil that are measured and calculated. The corresponding impedance is calculated and given below the current and voltage pulses. Only one capacitors bank has been used, with initial voltage from *2500 V* to *7500 V* (V_0 *= 2.5 / 3.5 / 4.5 / 5.5 / 7.5 kV* respectively, i.e. *Energy = 0.86 / 1.2 / 1.55 / 1.9 / 2.58 kJ*), to stay below the plastic strain. Electrical features of the generator are given in the Appendix E.2. The model allows the computation of the transient pulses and of the impedance (R and $X=L\omega_n$) changeable when a deformation occurs. The linear assumption is confirmed by both the measurements and the computations: R and X do not depend on the voltage, but only on the changeable airgap g. This last dependence is very weak with small elastic deformation but might become more significant with strong plastic deformation. The general decaying oscillating shape of both the current and the voltage is correctly described, but still neglects high frequency disturbances mainly due to the spark gaps. Maximum values, natural periods and decaying factors are well found for the voltage and the current pulses, giving rise to the force pulse and hence a strain and the elastic deformation. **Figure 15** represents the surface Lorentz force density acting on the tube's external surface (**Figure 15**, LEFT) and the tube deformation (**Figure 15**, RIGHT) as a function of time during the first current pulse (from 0 to 13 μs). Despite a time-delay between the 1D or 2D model and the 3D model on both the force and the displacement, the peak values attained, the one responsible for the end forming state, are very similar. Results on the force are better than the ones for the displacement because the mechanical model does not take the 2D effects into account (around 5% error for the peak force and 25% error for the peak displacement).

5.2.3. Results with tube and plastic deformation

Now the five capacitors banks have been used, with an initial voltage of $V_0 = 5\ kV$, to attain the plastic strain but stay below the ultimate tensile strength. Both measurements and computations have been done with four field-shapers made of different materials (Steel, CuBe, Siclanic® and Cuprofor® @Le Bronze Alloys). Peak values and natural frequencies are correctly found for the current pulses (see). The final and most important result is the prediction of the end forming state shown in **Figure 17**. The model gives the end deformation with a final diameter which is at the lower limit measured on samples, with a weak over-estimation coherent with **Figure 15**.

Table 6: Current pulse needed and natural frequency with initial voltage $V_0 = 5\ kV$ (i.e. *8.6 kJ* from generator) for various field-shapers' material.

Material	Method	I_{peak} *(kA)*	*f (Hz)*
Steel	Model	**320**	**20250**
8 % IACS	Meas.	**340**	**20500**
CuBe	Model	**340**	**21315**
25 % IACS	Meas.	**360**	**21700**
Siclanic®	Model	**350**	**21700**
46 % IACS	Meas.	**370**	**21800**
Cuprofor®	Model	**355**	**21975**
85 % IACS	Meas.	**375**	**21900**

5.3. Forecasting, Energy Balance sheet and discussions

Thanks to coupled models, the model can be an interesting forecasting tool for the forming and crimping processes in industrial applications (see **Figure 17**). Raoelison et al. (2012) proposed something similar by analysing the conditions for an efficient welding process. Cui et al. (2016) carried out a sensitivity analysis of the magnetic pulse welding as a function of the tube thickness. The present tool can be used to estimate the energy balance and the global efficiency of the process as shown in **Figure 16**, with possibilities to vary geometrical, physical and process parameters for optimisation purposes. The aim is to enhance the mechanical energy used to form the tube, *i.e.* to change from the initial diameter to the end lower diameter. This can help the design of efficient coils and flux concentrators for pulsed high magnetic fields like in Wilson and Srivastava (1965) but taking the whole geometry and process into account.

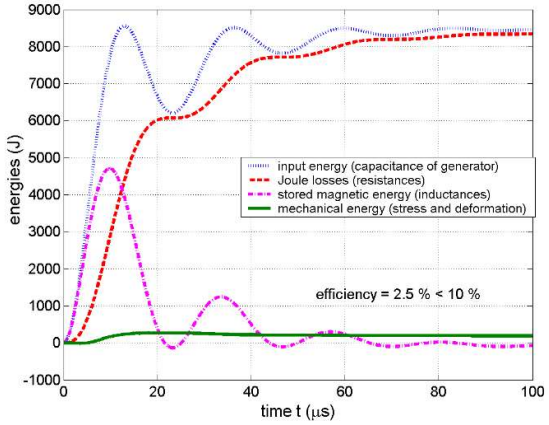

Figure 16. Energy balance with initial voltage $V_0 = 5\ kV$ (i.e. total energy 8.6 kJ from generator) for the field-shaper made with the Cuprofor® material.

6. Conclusion and perspectives

In this paper, we propose an analytical modelling of the 1-turn bulk coil with a cut, made of conducting steel or copper alloys, and used in the magneto-forming processing technology. The basic electromagnetic theory is first summarised and the One-Dimensional (1-D) axi-symmetrical approximation is discussed (part 2). The goal is to be able to determine the magnetic vector potential ***A*** diffusion that

will lead to all the interesting parameters sought to characterise, qualify, feed and optimize the use of the coil. The pseudo-harmonic solution to the 1D-problem is expanded with the help of Bessel basis functions, including some specific limit conditions and constraints (part 3). It is shown that it is then possible to estimate with reasonable time and accuracy the main coils parameters, that are electromagnetic (magnetic field, flux and current densities), magnetic (magnetic energy, equivalent inductance), electrical (energy loss, equivalent resistance) and mechanical (maximum Lorentz force density, self and mutual coefficients). The results obtained from calculations are compared to numerical 2-D and 3-D computations performed thanks to the Finite Element Method in certain test cases with and without a tube, which will be shaped. Significant discrepancies due to the 2D effects are compensated thanks to a 2D correction factor determined by FEM simulations. Moreover, as long as the frequency is high enough to give a skin depth very small compared to the coil radius, the proposed model does not only give the final numerical value of each characteristic, but it also provides complete analytical formulae, with explicit dependences upon some key geometrical and physical input variables (such as the changeable air gap between the coil and the tube, linked to the deformation). The use of a pseudo harmonic working condition is justified by comparing it to the transient working condition for which the model is improved and experimental measurements are carried out with and without a tube but with no deformation (part 4). The results are close and coherent with each other when performing an equivalent electrical circuit and the electro-mechanical coupling solution, which can be used with deformation in the transient working conditions (part 5). This model might ease either the transient calculation or the coupling with electrical and mechanical physics. It takes up less memory space, is less time consuming and above all it allows us to quickly estimate the main coil parameters and so optimise its conception (geometry, materials). It has been used in this paper to forecast the end deformation of a tube but should be developed to contribute to estimate the damaging strain and deformation, aging and life time of a field-shaper and a coil.

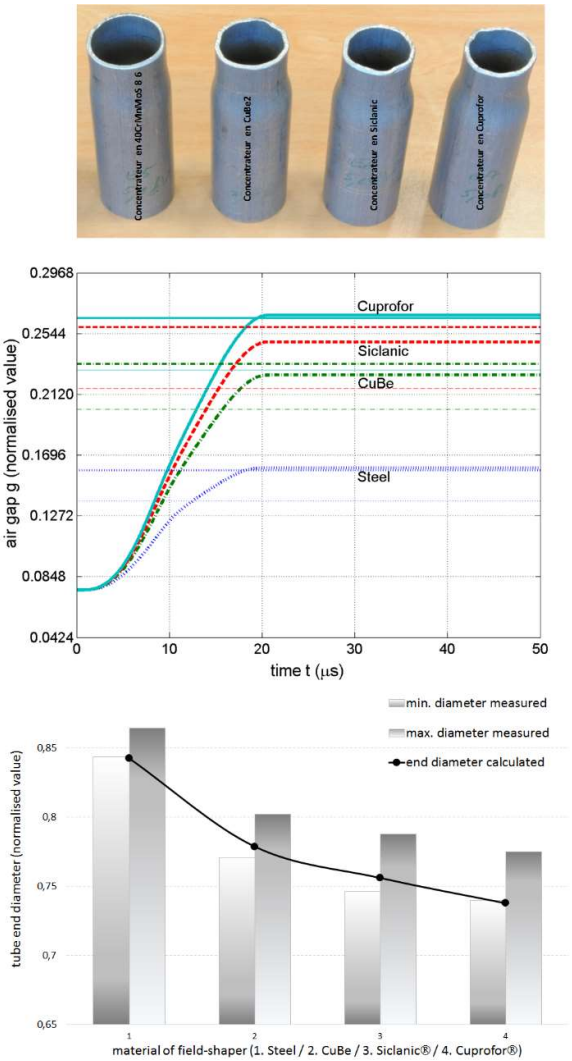

Figure 17. End deformation with $V_0 = 5\ kV$ and various field-shapers @Le Bronze Alloys. Comparison with measurements @ PFT Innovaltech.

Acknowledgments

We express our gratitude to the Picardie Region who gave financial support to this work under the project “COILTIM”.

Bibliography

(Arnaud et al., 1985) D. Arnaud, J. Barbery, R. Biais, B. Fargette, P. Naudot, *Propriétés du cuivre et de ses alliages*, Technique de l’Ingénieur, 1985, 10th of April, Article / Réf : M4640 v1.

(Conway, 2001) J.T. Conway, *Exact Solutions for the Magnetic Fields of Axisymmetric Solenoids and Current Distributions*, IEEE Transactions on Magnetics, 2001, Vol. 37, Issue no. 4, pp 2977 – 2988.

(Conway, 2007) J.T. Conway, *Inductance calculations for nonaxial coils using Bessel functions*, IEEE Transactions on Magnetics, 2007, Vol. 43, Issue no. 3, pp 1023 – 1034.

(Cui et al., 2016) J. Cui, G. Sun, J. Xu, Z. Xu, X. Huang, *A study on the critical wall thickness of the inner tube for magnetic pulse welding of tubular Al-Fe parts*, Journal of Materials Processing Technology, 2016, Vol. 227, pp 138 – 146.

(Daehn et al., 2008) G.S. Daehn, Y. Zhang, S. Golowin, K. Banik, A. Vivek, J.R. Johnson, G. Taber, G.K. Fenton, I. Henchi, P. L’Eplattenier, *Coupling Experiment and Simulation in Electromagnetic Forming Using Photon Doppler Velocimetry*, 3rd international Conference on High Speed Forming, 2008.

(Dodd and Deeds, 1968) C. V. Dodd, and W. E. Deeds, *Analytical Solutions to Eddy-Current Probe-Coil Problems*, Journal of Applied Physics, 1968, Vol. 39, pp 2829.

(Dodd, 1967) C. V. Dodd, *A Solution to Electromagnetic Induction Problems*, M. S. Thesis, University of Tennessee, Oak Ridge National Laboratory, 1967.

(Figueiredo and Laks, 1989) R. Figueiredo Jardim, B. Laks, *Kelvin functions for determination of magnetic susceptibility in nonmagnetic metals*, Journal of Applied Physics, 1989, 15 June, Vol. 65, Issue no. 12.

(Gray and Mathews, 1985) Andrew Gray, G. B. Mathews, *A treatise on Bessel functions and their applications to physics*, Macmillan and co. and New York. 1985.

(Guglielmetti, 2012) A. Guglielmetti, *Etude numérique du soudage par impulsion magnétique*, 2012, PhD thesis, UTC Compiègne, France.

(Hahn et al., 2016) M. Hahn, C. Weddeling, J. Lueg-Althoff, A.E. Tekkaya, *Analytical approach for magnetic pulse welding of sheet connections*, Journal of Materials Processing Technology, 2016, Vol. 230, pp 131 – 142.

(Jablonski and Winkler, 1978) J. Jablonski, R. Winkler, *Analysis of the electromagnetic forming process*, Int. J. Mech. Sci. Pergamon Press., 1978, Vol. 20, pp. 315-325.

(Johnson and Cook, 1983) G. Johnson, W. Cook, *A constitutive model and data for metals subjected to large strains, high strain rates and high temperatures*, Proceedings of the 7th international symposium on ballistics, Hague, Netherlands, 1983, pp 541 – 547.

(Kinsey and Nassiri, 2017) B. Kinsey, A. Nassiri, *Analytical model and experimental investigation of electromagnetic tube compression with axi-symmetric coil and field-shaper*, CIRP Annals – Manufacturing technology, 2017, Vol. 66, pp 273 – 276.

(Labinac et al., 2006) V. Labinac, N. Erceg, D. Kotnik-Karuza, *Magnetic field of a cylindrical coil*, American Journal of Physics, 2006, Vol. 74, pp 621 – 627.

(Lal and Hillier, 1968) G. K. Lal, M. J. Hillier, *The electrodynamics of electromagnetic forming*, Int. J. Mech. Sci. Pergamon Press., 1968, Vol. 10, pp. 491-500.

(Lockyer and Noble, 1999) S.A. Lockyer, F.W. Noble, *Fatigue of precipitate strengthened Cu-Ni-Si alloy*, Materials Science and Technology, 1999, Vol. 15, pp. 1147.

(Maloberti et al., 2015) O. Maloberti, O. Mansouri, D. Jouaffre, D. Haye, *Harmonic and Transient Magnetic analysis of Single Turn Coils fed by a Current Pulse at Medium Frequency*, COMSOL Conference, 2015, 14-16 october, Grenoble.

(Mansouri et al., 2016) O. Mansouri, O. Maloberti, D. Jouaffre, M. Hamzaoui, J. Derosière, D. Haye, J.P. Leonard, P. Pelca, *Analytical calculation of a 1-turn coil parameters for the magneto-forming technology*, ICHSF Conference, 2016, 27-28th of April, Dortmund.

(Nassiri et al., 2015) A. Nassiri, C. Campbeli, G. Chini, B. Kinsey, *Analytical model and experimental validation of single-turn, axi-symmetric coil for electromagnetic forming and welding*, Procedia Manufacturing, 2015, Vol. 1, pp 814 – 827.

(Otin et al., 2011) R. Otin, R. Mendez, O. Fruitos, *A numerical model for the search of the optimum capacitance in electromagnetic metal forming*, American Institute of Physics, AIP Conf. Proc., 2011, Vol. 1383, pp 935 – 942.

(Psyk et al., 2011) V. Psyk, D. Risch, B. L. Kinsey, A. E. Tekkaya, M. Kleiner, 2011, *Electromagnetic Forming – A review,* Journal of Materials Processing Technology, 2011, Vol. 211, pp 787 – 829.

(Raoelison et al., 2012) R.N. Raoelison, N. Buiron, M. Rachik, D. Haye, G. Franz, *Efficient welding conditions in magnetic pulse welding process, Journal of Manufacturing Processes*, 2012, Vol. 14, pp 372 – 377.

(Ravaud et al., 2010) R. Ravaud, G. Lemarquand, V. Lemarquand, S. Babic, C. Akyel, *Mutual inductance and force exerted between thick coils,* Progress in Electromagnetics Research, 2010, Vol. 102, pp 367 – 380.

(Sapanathan et al., 2015) T. Sapanathan, K. Yang, N. Buiron, M. Rachik, “*Insight into the realistic behaviours of magnetic pulse forming and welding processes using numerical simulations*, I²FG Impulse Forming Workshop, 2015, October, Dortmund, Germany.

(Shang et al., 2012) J. Shang, S. Hatkevich, L. Wilkerson, *Experimental Study and Numerical Simulation of Electromagnetic Tube Expansion*, 5th International Conference on High Speed Forming, 2012, pp. 83 – 92.

(weddeling et al., 2015) C. Weddeling, O. K. Demir, P. Haupt, A. E. Tekkaya, *Analytical methodology for the process of electromagnetic crimping*, Journal of Materials Processing Technology, 2015, August, Vol. 222, pp 163 – 180.

(Wilson and Srivastava, 1965) M. N. Wilson, K. D. Srivastava, *Design of Efficient Flux Concentrators for Pulsed High Magnetic Fields*, The Review of Scientific Instruments, 1965, August, Vol. 36, Issue no. 8.

(Yu and Han, 1987) D. Yu, K.S. Han, *Self-Inductance of Air-Core Circular Coils with rectangular cross section*, IEEE Transactions on Magnetics, 1987, Vol. MAG-23, Issue no. 6, pp 3916 – 3921.

Appendix A Initial data

A.1 The coil geometry (TEST CASE 1)

Table 7: *Parameters of the coil geometry of Test-Case 1.*

Name	Value	significance
R_{1i}	17.5 mm	internal tube radius
R_{1e}	19 mm	external tube radius
g_2	1 mm	airgap between coil and tube
R_{3i}	20 mm	internal coil radius
R_{3ie}	30 mm	intermediate coil radius
R_{3e}	100 mm	external coil radius
Z	30 mm	useful length of coil
Z_t	50 mm	total end length of coil

A.2 The materials (TEST CASE 1)

Table 8: *Parameters of the materials (@20°C) of Test-Case 1.*

Name	Value	significance
μ_0	$4\pi.10^{-7}$ H.m^{-1}	Air magnetic permeability
σ_1	75 % IACS*	Tube electrical conductivity
μ_1	μ_0	Tube magnetic permeability
σ_3	10 % IACS*	Coil electrical conductivity
μ_3	μ_0	Coil magnetic permeability
σ_{Cu}	5.8 10^7 S.m^{-1}	Copper conductivity

*IACS: International Annealed Copper Standard (100 % = σCu)

Appendix B Solutions

B.1 Total magnetic vector potential

For each conducting region k, the total magnetic vector potential will be of the following form:

$$A_k(r,\omega) = C_k J_1(\alpha_{1k} r) + D_k Y_1(\alpha_{1k} r) \quad \text{(a1)}$$

$$B_k(r,\omega) = C_k \alpha_{1k} J_0(\alpha_{1k} r) + D_k \alpha_{1k} Y_0(\alpha_{1k} r) \quad \text{(a2)}$$

$$j_k(r,\omega) = -i\sigma_k \omega C_k J_1(\alpha_{1k} r) - i\sigma_k \omega D_k Y_1(\alpha_{1k} r) \quad \text{(a3)}$$

$$f_k(r) = real\left(j_k(r) B_k^*(r)\right) \quad \text{(a4)}$$

$$\sigma_{bk}(r) = -\frac{B_k(r) B_k^*(r)}{2\mu_k} \quad \text{(a5)}$$

We use ΔJ_{0k} and ΔY_{0k} for $k=1$ and $k=3$ defined by:

$$\Delta J_{0k} = J_0(\alpha_{1k} R_{ke}) - J_0(\alpha_{1k} R_{ki}) \quad \text{(a6)}$$

$$\Delta Y_{0k} = Y_0(\alpha_{1k} R_{ke}) - Y_0(\alpha_{1k} R_{ki}) \quad \text{(a7)}$$

In each region k, the coefficients C_k and D_k are proportional to (I/Z) and can be written as follows (C_k and D_k have got the same unit as the potential A [T.m] and K_{Ck} and K_{Dk} have got the same unit as an inductance L [H]).

$$C_k = K_{Ck}\left(\frac{I}{Z}\right) \quad \text{(a8) and} \quad D_k = K_{Dk}\left(\frac{I}{Z}\right) \quad \text{(a9)}$$

B.1.1 Coil on its own

Region 1: the coil

$$K_{C1} = \sqrt{\frac{\mu_1}{\sigma_1 \omega}}\left(\frac{Z}{Z_1}\right)\frac{\left[\left(\frac{\alpha_2}{\alpha}\right)Y_0(\alpha_1 R_{1i}) - \left(\frac{\alpha}{\alpha_1}\right)\Delta Y_{01}\right]}{\left[Y_0(\alpha_1 R_{1i})\Delta J_{01} - J_0(\alpha_1 R_{1i})\Delta Y_{01}\right]} \quad \text{(a10)}$$

$$K_{D1} = \sqrt{\frac{\mu_1}{\sigma_1 \omega}}\left(\frac{Z}{Z_1}\right)\frac{\left[-\left(\frac{\alpha_2}{\alpha}\right)J_0(\alpha_1 R_{1i}) + \left(\frac{\alpha}{\alpha_1}\right)\Delta J_{01}\right]}{\left[Y_0(\alpha_1 R_{1i})\Delta J_{01} - J_0(\alpha_1 R_{1i})\Delta Y_{01}\right]} \quad \text{(a11)}$$

B.1.2 Coil with tube

Region 1: the tube

Region 3: the coil

$$K_{C3} = \sqrt{\frac{\mu_3}{\sigma_3 \omega}}\left(\frac{Z}{Z_3}\right)\frac{\left[\left(\frac{a_{23}}{a_3}\right)Y_0(\alpha_{13} R_{3i}) - (1+\beta)\left(\frac{a_3}{a_{13}}\right)\Delta Y_{03}\right]}{\left[Y_0(\alpha_{13} R_{3i})\Delta J_{03} - J_0(\alpha_{13} R_{3i})\Delta Y_{03}\right]} \quad \text{(a12)}$$

$$K_{D3} = \sqrt{\frac{\mu_3}{\sigma_3 \omega}}\left(\frac{Z}{Z_3}\right)\frac{\left[-\left(\frac{a_{23}}{a_3}\right)J_0(\alpha_{13} R_{3i}) + (1+\beta)\left(\frac{a_3}{a_{13}}\right)\Delta J_{03}\right]}{\left[Y_0(\alpha_{13} R_{3i})\Delta J_{03} - J_0(\alpha_{13} R_{3i})\Delta Y_{03}\right]} \quad \text{(a13)}$$

$$K_{C1} = \sqrt{\frac{\mu_1}{\sigma_1 \omega}}\left(\frac{Z}{Z_1}\right)\frac{\left[\beta\left(\frac{a_{21}}{a_1}\right)Y_0(\alpha_{11} R_{1e}) - (1+\beta)\left(\frac{a_1}{a_{11}}\right)\Delta Y_{01}\right]}{\left[-Y_0(\alpha_{11} R_{1e})\Delta J_{01} - J_0(\alpha_{11} R_{1e})\Delta Y_{01}\right]} \quad \text{(a14)}$$

$$K_{D1} = \sqrt{\frac{\mu_1}{\sigma_1 \omega}}\left(\frac{Z}{Z_1}\right)\frac{\left[\beta\left(\frac{a_{21}}{a_1}\right)J_0(\alpha_{11} R_{1e}) + (1+\beta)\left(\frac{a_1}{a_{11}}\right)\Delta J_{01}\right]}{\left[Y_0(\alpha_{11} R_{1e})\Delta J_{01} + J_0(\alpha_{11} R_{1e})\Delta Y_{01}\right]} \quad \text{(a15)}$$

B.1.3 Coil with field-shaper and tube

Region 1: the tube

Region 3: the field-shaper

Region 5: the coil

$$K_{C5} = \sqrt{\frac{\mu_5}{\sigma_5 \omega}}\left(\frac{Z}{Z_5}\right)\frac{\left[\left(\frac{a_{25}}{a_5}\right)Y_0(\alpha_{15} R_{5i}) - (1+\beta_{35})\left(\frac{a_5}{a_{15}}\right)\Delta Y_{05}\right]}{\left[Y_0(\alpha_{15} R_{5i})\Delta J_{05} - J_0(\alpha_{15} R_{5i})\Delta Y_{05}\right]} \quad \text{(a16)}$$

$$K_{D5} = \sqrt{\frac{\mu_5}{\sigma_5 \omega}}\left(\frac{Z}{Z_5}\right)\frac{\left[-\left(\frac{a_{25}}{a_5}\right)J_0(\alpha_{15} R_{5i}) + (1+\beta_{35})\left(\frac{a_5}{a_{15}}\right)\Delta J_{05}\right]}{\left[Y_0(\alpha_{15} R_{5i})\Delta J_{05} - J_0(\alpha_{15} R_{5i})\Delta Y_{05}\right]} \quad \text{(a17)}$$

$$K_{C35} = \sqrt{\frac{\mu_3}{\sigma_3 \omega}}\left(\frac{Z}{Z_{35}}\right)\frac{\left[\beta_{35}\left(\frac{a_{23}}{a_3}\right)Y_0(\alpha_{13} R_{3e}) - (1+\beta_{35})\left(\frac{a_3}{a_{13}}\right)\Delta Y_{03}\right]}{\left[-Y_0(\alpha_{13} R_{3e})\Delta J_{03} - J_0(\alpha_{13} R_{3e})\Delta Y_{03}\right]} \quad \text{(a18)}$$

$$K_{D35} = \sqrt{\frac{\mu_3}{\sigma_3 \omega}}\left(\frac{Z}{Z_{35}}\right)\frac{\left[\beta_{35}\left(\frac{a_{23}}{a_3}\right)J_0(\alpha_{13} R_{3e}) + (1+\beta_{35})\left(\frac{a_3}{a_{13}}\right)\Delta J_{03}\right]}{\left[Y_0(\alpha_{13} R_{3e})\Delta J_{03} + J_0(\alpha_{13} R_{3e})\Delta Y_{03}\right]} \quad \text{(a19)}$$

$$K_{C31} = \sqrt{\frac{\mu_3}{\sigma_3 \omega}}\left(\frac{Z}{Z_{31}}\right)\frac{\left[\left(\frac{a_{23}}{a_3}\right)Y_0(\alpha_{13} R_{3i}) - (1+\beta_{31})\left(\frac{a_3}{a_{13}}\right)\Delta Y_{03}\right]}{\left[Y_0(\alpha_{13} R_{3i})\Delta J_{03} - J_0(\alpha_{13} R_{3i})\Delta Y_{03}\right]}(\beta_{35}) \quad \text{(a20)}$$

$$K_{D31} = \sqrt{\frac{\mu_3}{\sigma_3 \omega}}\left(\frac{Z}{Z_{31}}\right)\frac{\left[-\left(\frac{a_{23}}{a_3}\right)J_0(\alpha_{13} R_{3i}) + (1+\beta_{31})\left(\frac{a_3}{a_{13}}\right)\Delta J_{03}\right]}{\left[Y_0(\alpha_{13} R_{3i})\Delta J_{03} - J_0(\alpha_{13} R_{3i})\Delta Y_{03}\right]}(\beta_{35}) \quad \text{(a21)}$$

$$K_{C1} = \sqrt{\frac{\mu_1}{\sigma_1 \omega}}\left(\frac{Z}{Z_1}\right)\frac{\left[\beta_{31}\left(\frac{a_{21}}{a_1}\right)Y_0(\alpha_{11} R_{1e}) - (1+\beta_{31})\left(\frac{a_1}{a_{11}}\right)\Delta Y_{01}\right]}{\left[-Y_0(\alpha_{11} R_{1e})\Delta J_{01} - J_0(\alpha_{11} R_{1e})\Delta Y_{01}\right]}(\beta_{35}) \quad \text{(a22)}$$

$$K_{D1} = \sqrt{\frac{\mu_1}{\sigma_1 \omega}}\left(\frac{Z}{Z_1}\right)\frac{\left[\beta_{31}\left(\frac{a_{21}}{a_1}\right)J_0(\alpha_{11} R_{1e}) + (1+\beta_{31})\left(\frac{a_1}{a_{11}}\right)\Delta J_{01}\right]}{\left[Y_0(\alpha_{11} R_{1e})\Delta J_{01} + J_0(\alpha_{11} R_{1e})\Delta Y_{01}\right]}(\beta_{35}) \quad \text{(a23)}$$

B.2 Reduced magnetic vector potential

For each region k, the reduced magnetic vector potential will be of the following form in air, in conducting regions with no source and in conducting regions with a source respectively:

$$A_{ik}(r) = C_k r + \frac{D_k}{r} \quad \text{(b1)}$$

$$A_{ik}(r,\omega) = C_k J_1(\alpha_{1k} r) + D_k Y_1(\alpha_{1k} r) \quad \text{(b2)}$$

$$A_{ik}(r,\omega) = \left(C_k + \frac{\mu_k \sigma_k \Delta V}{4\alpha_{1k}}\left(Y_0(\alpha_{1k} r) - Y_0(\alpha_{1k} R_{ki})\right)\right) J_1(\alpha_{1k} r) + \left(D_k - \frac{\mu_k \sigma_k \Delta V}{4\alpha_{1k}}\left(J_0(\alpha_{1k} r) - J_0(\alpha_{1k} R_{ki})\right)\right) Y_1(\alpha_{1k} r) \quad \text{(b3)}$$

B.2.1 Coil on its own

Region 0 = the interior air; Region 1 = the coil

$$\begin{bmatrix} R_{1i} & -J_1(\alpha_{11}R_{1i}) & -Y_1(\alpha_{11}R_{1i}) \\ 2\mu_1/\mu_0 & -\alpha_{11}J_0(\alpha_{11}R_{1i}) & -\alpha_{11}Y_0(\alpha_{11}R_{1i}) \\ 2(Z_0/Z_1)/\mu_0 & -i(\sigma_1\omega/\alpha_{11})\Delta J_{01} & -i(\sigma_1\omega/\alpha_{11})\Delta Y_{01} \end{bmatrix} \begin{pmatrix} C_0 \\ C_1 \\ D_1 \end{pmatrix} = \begin{pmatrix} 0 \\ 0 \\ K_1(\Delta V) \end{pmatrix} \quad \text{(b4)}$$

$$K_1(\Delta V) = \sigma_1 \Delta V \left(\frac{Z}{Z_1}\right)\left(-\frac{1}{2\pi} ln(R_{1e}/R_{1i}) + \frac{i}{4}\left(J_0(\alpha_{11}R_{1i})\Delta Y_{01} - Y_0(\alpha_{11}R_{1i})\Delta J_{01}\right)\right) \quad \text{(b5)}$$

B.2.2 Coil with tube

Region 0 = the interior air; Region 1 = the tube; Region 2 = the airgap between the coil and the tube; Region 3 = the coil

$$\begin{bmatrix} R_{1i} & -J_1(\alpha_{11}R_{1i}) & -Y_1(\alpha_{11}R_{1i}) & 0 & 0 & 0 & 0 & 0 \\ 2\mu_1/\mu_0 & -\alpha_{11}J_0(\alpha_{11}R_{1i}) & -\alpha_{11}Y_0(\alpha_{11}R_{1i}) & 0 & 0 & 0 & 0 & 0 \\ -2Z_0\mu_1/\mu_0 & \alpha_{11}Z_1J_0(\alpha_{11}R_{1e}) & \alpha_{11}Z_1Y_0(\alpha_{11}R_{1e}) & 0 & 0 & 0 & 0 & \mu_1 \\ 0 & J_1(\alpha_{11}R_{1e}) & Y_1(\alpha_{11}R_{1e}) & -R_{1e} & -1/R_{1e} & 0 & 0 & 0 \\ 0 & \alpha_{11}J_0(\alpha_{11}R_{1e}) & \alpha_{11}Y_0(\alpha_{11}R_{1e}) & -2\mu_1/\mu_2 & 0 & 0 & 0 & 0 \\ 0 & 0 & 0 & R_{3i} & 1/R_{3i} & -J_1(\alpha_{13}R_{3i}) & -Y_1(\alpha_{13}R_{3i}) & 0 \\ 0 & 0 & 0 & 2\mu_3/\mu_2 & 0 & -\alpha_{13}J_0(\alpha_{13}R_{3i}) & -\alpha_{13}Y_0(\alpha_{13}R_{3i}) & 0 \\ 0 & 0 & 0 & 2(Z_2/Z_3)/\mu_2 & 0 & -i(\sigma_3\omega/\alpha_{13})\Delta J_{03} & -i(\sigma_3\omega/\alpha_{13})\Delta Y_{03} & 0 \end{bmatrix} \begin{pmatrix} C_0 \\ C_1 \\ D_1 \\ C_2 \\ D_2 \\ C_3 \\ D_3 \\ -I_1 \end{pmatrix} = \begin{pmatrix} 0 \\ 0 \\ 0 \\ 0 \\ 0 \\ 0 \\ 0 \\ K_3(\Delta V) \end{pmatrix} \quad \text{(b6)}$$

$$K_3(\Delta V) = \sigma_3 \Delta V \left(\frac{Z}{Z_3}\right)\left(-\frac{1}{2\pi} ln(R_{3e}/R_{3i}) + \frac{i}{4}\left(J_0(\alpha_{13}R_{3i})\Delta Y_{03} - Y_0(\alpha_{13}R_{3i})\Delta J_{03}\right)\right) \quad \text{(b7)}$$

B.2.3 Coil with field-shaper and tube

Region 1 = the tube; Region 3 = the field-shaper; Region 5 = the coil

$$\begin{bmatrix} R_{1i} & -J_1(\alpha_{11}R_{1i}) & -Y_1(\alpha_{11}R_{1i}) & & & & & \\ 2\mu_1/\mu_0 & -\alpha_{11}J_0(\alpha_{11}R_{1i}) & -\alpha_{11}Y_0(\alpha_{11}R_{1i}) & 0 & 0 & 0 & 0 & 0 \\ -2Z_0\mu_1/\mu_0 & \alpha_{11}Z_1J_0(\alpha_{11}R_{1e}) & \alpha_{11}Z_1Y_0(\alpha_{11}R_{1e}) & 0 & 0 & 0 & 0 & \mu_1 \\ 0 & J_1(\alpha_{11}R_{1e}) & Y_1(\alpha_{11}R_{1e}) & -R_{1e} & -1/R_{1e} & 0 & 0 & 0 \\ 0 & \alpha_{11}J_0(\alpha_{11}R_{1e}) & \alpha_{11}Y_0(\alpha_{11}R_{1e}) & 2\mu_1/\mu_2 & 0 & 0 & 0 & 0 \\ 0 & 0 & 0 & R_{1i} & 1/R_{1i} & -J_1(\alpha_{13}R_{3li}) & -Y_1(\alpha_{13}R_{3li}) & 0 \\ 0 & 0 & 0 & 2\mu_3/\mu_2 & 0 & -\alpha_{13}J_0(\alpha_{13}R_{3li}) & -\alpha_{13}Y_0(\alpha_{13}R_{3li}) & 0 \\ 0 & 0 & 0 & 2(Z_2/Z_3)/\mu_2 & 0 & -i(\sigma_3\omega/\alpha_{13})\Delta J_{031} & -i(\sigma_3\omega/\alpha_{13})\Delta Y_{031} & 0 \end{bmatrix} \begin{pmatrix} C_0 \\ C_1 \\ D_1 \\ C_2 \\ D_2 \\ C_{31} \\ D_{31} \\ -I_1 \end{pmatrix} = \begin{pmatrix} 0 \\ 0 \\ 0 \\ 0 \\ 0 \\ 0 \\ 0 \\ K_{31}(\Delta V) \end{pmatrix} \quad \text{(b8)}$$

$$\begin{bmatrix} -J_1(\alpha_{13}R_{35i}) & -Y_1(\alpha_{13}R_{35i}) & 0 & 0 & 0 & 0 & 0 \\ Z_4\alpha_{13}\Delta J_{035} & Z_4\alpha_{13}\Delta Y_{035} & 0 & 0 & 0 & 0 & \mu_3 \\ J_1(\alpha_{13}R_{35e}) & Y_1(\alpha_{13}R_{35e}) & -R_{35e} & -1/R_{35e} & 0 & 0 & 0 \\ \alpha_{13}J_0(\alpha_{13}R_{35e}) & \alpha_{13}Y_0(\alpha_{13}R_{35e}) & -2\mu_3/\mu_4 & 0 & 0 & 0 & 0 \\ 0 & 0 & R_{5i} & -1/R_{5i} & -J_1(\alpha_{15}R_{5i}) & -Y_1(\alpha_{15}R_{5i}) & 0 \\ 0 & 0 & 2\mu_5/\mu_4 & 0 & -\alpha_{15}J_0(\alpha_{15}R_{5i}) & -\alpha_{15}Y_0(\alpha_{15}R_{5i}) & 0 \\ 0 & 0 & 2(Z_4/Z_5)/\mu_4 & 0 & -i(\sigma_5\omega/\alpha_{15})\Delta J_{05} & -i(\sigma_5\omega/\alpha_{15})\Delta Y_{05} & 0 \end{bmatrix} \begin{pmatrix} C_{35} \\ D_{35} \\ C_4 \\ D_4 \\ C_5 \\ D_5 \\ -I_3 \end{pmatrix} = \begin{pmatrix} 0 \\ 0 \\ 0 \\ 0 \\ 0 \\ 0 \\ K_5(\Delta V) \end{pmatrix} \quad \text{(b9)}$$

$$K_{31}(\Delta V) = \sigma_3 \Delta V \left(\frac{Z}{Z_3}\right)\left(-\frac{1}{2\pi} ln(R_{31e}/R_{31i}) + \frac{i}{4}\left(J_0(\alpha_{13}R_{31i})\Delta Y_{031} - Y_0(\alpha_{13}R_{31i})\Delta J_{031}\right)\right) \quad \text{(b10)}$$

$$K_5(\Delta V) = \sigma_5 \Delta V \left(\frac{Z}{Z_5}\right)\left(-\frac{1}{2\pi} ln(R_{5e}/R_{5i}) + \frac{i}{4}\left(J_0(\alpha_{15}R_{5i})\Delta Y_{05} - Y_0(\alpha_{15}R_{5i})\Delta J_{05}\right)\right) \quad \text{(b11)}$$

Appendix C Parameters

The local potential, fields and densities can be built with the Bessel functions. These must be calculated for a reference radius small enough (R_{ref} = *5* or *10 mm*) in order to make the matrix system solutions converge. We use an affinity transformation on the radial position: $r \rightarrow r(R_{ref}/R)$. The current source is unchanged but the voltage become $\Delta V \rightarrow \Delta V(R_{ref}/R)$. Then, thanks to the properties of Bessel functions and the skin depth of the material, the functions obtained with the reference radius can simply be moved as a function of the actual radius of the tube, the field-shaper or the coil, obtained by the affinity transformation.

Global performance parameters such as the induction and force coefficients or the inductance and the resistance can be determined either with the exact Bessel functions or its approximations given by (c1) and (c2), providing that $\alpha r >> 1$.

$$\begin{cases} J_1(\alpha_1 r) \sim \sqrt{\frac{2}{\pi\alpha_1 r}}\cos\left(\alpha_1 r - \frac{3\pi}{4}\right) \\ Y_1(\alpha_1 r) \sim \sqrt{\frac{\pi}{2\alpha_1 r}}\sin\left(\alpha_1 r - \frac{3\pi}{4}\right) \\ I_1(\alpha_1 r) \sim \sqrt{\frac{1}{2\pi\alpha_1 r}}\exp(\alpha_1 r) \\ K_1(\alpha_2 r) \sim \sqrt{\frac{\pi}{2\alpha_2 r}}\exp(-\alpha_2 r) \end{cases} \quad (c1)$$

$$\begin{cases} J_0(\alpha_1 r) \sim \sqrt{\frac{2}{\pi\alpha_1 r}}\cos\left(\alpha_1 r - \frac{\pi}{4}\right) \\ Y_0(\alpha_1 r) \sim \sqrt{\frac{\pi}{2\alpha_1 r}}\sin\left(\alpha_1 r - \frac{\pi}{4}\right) \\ I_0(\alpha_1 r) \sim \sqrt{\frac{1}{2\pi\alpha_1 r}}\exp(\alpha_1 r) \\ K_0(\alpha_2 r) \sim \sqrt{\frac{\pi}{2\alpha_2 r}}\exp(-\alpha_2 r) \end{cases} \quad (c2)$$

C.1 Resistances

For each conducting region *k=2p+1*

$$R_k \approx \frac{2\sigma_k\omega^2 Z_k}{|\alpha_k|Z^2}\left(\begin{array}{l} \left[\frac{\sin((\alpha_{1k}+\alpha_{2k})r)}{\alpha_{1k}+\alpha_{2k}}\right]_{R_{ki}}^{R_{ke}}(K_{ck}^2+K_{Dk}^2)+ \\ \left[\frac{\cos((\alpha_{1k}-\alpha_{2k})r)}{\alpha_{1k}-\alpha_{2k}}\right]_{R_{ki}}^{R_{ke}}(K_{ck}^2-K_{Dk}^2)+ \\ \left[\frac{\cos((\alpha_{1k}+\alpha_{2k})r)}{\alpha_{1k}+\alpha_{2k}}\right]_{R_{ki}}^{R_{ke}}(K_{Ck}K_{Dk}^*-K_{Ck}^*K_{Dk})+ \\ \left[\frac{\sin((\alpha_{1k}-\alpha_{2k})r)}{\alpha_{1k}-\alpha_{2k}}\right]_{R_{ki}}^{R_{ke}}(K_{Ck}K_{Dk}^*+K_{Ck}^*K_{Dk}) \end{array}\right) \quad (c3)$$

C.2 Inductances

For each air region *k=2p*

$$L_{k=2p} \approx \pi\left(R_{(k+1)i}^2 - R_{(k-1)e}^2\right)\frac{\mu_{k+1}^2 Z_k}{\mu_k Z_{k+1}^2} \quad (c4)$$

The magnetic energy stored in air regions is proportional to the coil magnetic permeability and the surface of flux in air.

For each conducting region *k=2p+1*

$$L_k \approx \frac{2Z_k}{\mu_k|\alpha_k|Z^2}\left(\begin{array}{l} \left[\frac{\sin((\alpha_{1k}+\alpha_{2k})r)}{\alpha_{1k}+\alpha_{2k}}\right]_{R_{ki}}^{R_{ke}}(K_{ck}^2+K_{Dk}^2)+ \\ \left[\frac{\cos((\alpha_{1k}-\alpha_{2k})r)}{\alpha_{1k}-\alpha_{2k}}\right]_{R_{ki}}^{R_{ke}}(-K_{ck}^2+K_{Dk}^2)+ \\ \left[\frac{\cos((\alpha_{1k}+\alpha_{2k})r)}{\alpha_{1k}+\alpha_{2k}}\right]_{R_{ki}}^{R_{ke}}(K_{Ck}K_{Dk}^*-K_{Ck}^*K_{Dk})- \\ \left[\frac{\sin((\alpha_{1k}-\alpha_{2k})r)}{\alpha_{1k}-\alpha_{2k}}\right]_{R_{ki}}^{R_{ke}}(K_{Ck}K_{Dk}^*+K_{Ck}^*K_{Dk}) \end{array}\right) \quad (c5)$$

C.3 Induction coefficient

C.3.1 Without field-shaper

Without tube: $K_{b0} \approx \mu_1\left(\frac{Z}{Z_1}\right)$ (c6)

With tube: $K_{b2} \approx (1+\beta)\mu_3\left(\frac{Z}{Z_3}\right)$ (c7)

C.3.2 With field-shaper

Without tube $K_{b0} \approx \beta_{35}\mu_3\left(\frac{Z}{Z_3}\right)$ (c8)

With tube: $K_{b2} \approx \beta_{35}(1+\beta_{13})\mu_3\left(\frac{Z}{Z_3}\right)$ (c9)

The unit of K_b is [H.m^{-1}]=[T/(A.m^{-1})].

(with $Z = Z_k$ for a semi-infinite coil or very large Z)

C.4 Force coefficients

C.4.1 Self-force onto the coil and field-shaper

For the coil or field-shaper region *k=1, 3 or 5*

$$K_{p(k=1,3,5)} \text{ or } K_{f(k=3)} \approx \left(\frac{\sigma_k K_{b(k-1)}\sqrt{2\omega}}{\sqrt{\pi\alpha_k R_{ki}}}\right)* Real\left(i\left(\begin{array}{l} K_{Ck}^* e^{i\frac{3\pi}{2}}\cos\left(\alpha_{2k}R_{ki}+\frac{3\pi}{4}\right)- \\ K_{Dk}^* e^{i\frac{3\pi}{2}}\sin\left(\alpha_{2k}R_{ki}+\frac{3\pi}{4}\right) \end{array}\right)\right) \quad (c10)$$

C.4.2 Mutual force onto the tube

For the tube region *k=1*

$$K_m \approx \left(\frac{\sigma_1 K_{b0}\sqrt{2\omega}}{\sqrt{\pi\alpha_1 R_{1e}}}\right)* Real\left(i\left(\begin{array}{l} K_{C1}^* e^{i\frac{3\pi}{2}}\cos\left(\alpha_{21}R_{1e}+\frac{3\pi}{4}\right)- \\ K_{D1}^* e^{i\frac{3\pi}{2}}\sin\left(\alpha_{21}R_{1e}+\frac{3\pi}{4}\right) \end{array}\right)\right) \quad (c11)$$

The unit of K_p, K_f and K_m is [H.m^{-2}.s$^{1/2}$]=[N.m^{-3}.s$^{1/2}$/(A.m^{-1})^2].

C.5 Maximum stress coefficient

For each conducting region *k=1, 3 or 5*

$$K_{sk} \approx \frac{K_{b(k-1)}^2}{\mu_k} = K_{b(k-1)}\left(\frac{Z}{Z_{k-1}}\right) \quad (c12)$$

Appendix D Simulations

D.1 Without field-shaper (*TESTCASE 1*)

D.1.1 The coil geometry

Table 9*: Parameters of the coil geometry of TESTCASE 1.*

Name	Value	significance
R_{1i}	17.5 mm	internal tube radius
R_{1e}	19 mm	external tube radius
$g=g_2$	1 mm	airgap between coil and tube
R_{3i}	20 mm	internal coil radius
R_{3ie}	30 mm	intermediate coil radius
R_{3e}	100 mm	external coil radius
Z	30 mm	useful length of coil
Z_t	50 mm	total length of coil

D.1.2 The materials

Table 10: *Parameters of the materials (@20°C) of TESTCASE 1.*

Name	Value	significance
σ_1	75 % IACS*	Tube electrical conductivity
μ_1	μ_0	Tube magnetic permeability
σ_3	10 % IACS*	Coil electrical conductivity
μ_3	μ_0	Coil magnetic permeability
E	210 GPa	Young modulus of tube
S_1	950 MPa	Johnson Cook coefficient 1
S_2	1250 MPa	Johnson Cook coefficient 2
S_3	0.083	Johnson Cook coefficient 3
n	0.43 n.u.	Johnson Cook exponent
ε_0'	1 %.s^{-1}	Reference speed

*IACS: International Annealed Copper Standard (100 % = σ_{Cu})

D.1.3 Other electrical parameters

Transient simulations are done superimposing the current pulse, *i.e.* its peak value I_{peak} and its natural frequency f_n. Pseudo-harmonic approximations are assumed.

Natural frequency: $f_n = 20\ kHz$

Peak current: $I_{peak} = 825\ kA$ (if Z = 30 mm)

Peak current: $I_{peak} = 825*Z[mm]/30\ kA$ (if Z ≠ 30 mm)

D.2 With field-shaper (*TESTCASE 2*)

D.2.1 The coil and field-shaper geometry

Table 11*: Parameters of the coil geometry of TESTCASE 2.*

Name	Value	significance
R_{1i}	17.5 mm	internal tube radius
R_{1e}	19 mm	external tube radius
$g=g_2$	1 mm	airgap between coil and tube
R_{3i}	20 mm	internal field-shaper radius
R_{3ie}	30 mm	mid field-shaper radius
R_{3e}	44.4 mm	external field-shaper radius
g_4	0.6 mm	airgap field-shaper - coil
R_{5i}	45 mm	internal coil radius
R_{5e}	100 mm	external coil radius
Z	30 mm	useful length of field-shaper
Z_t	50 mm	total length of coil

D.2.2 The materials

Table 12: *Parameters of the materials (@20°C) of TESTCASE 2.*

Name	Value	significance
σ_1	75 % IACS*	Tube electrical conductivity
μ_1	μ_0	Tube magnetic permeability
σ_3	50 % IACS*	Field-shaper conductivity
μ_3	μ_0	Field-shaper permeability
σ_5	10 % IACS*	Coil electrical conductivity
μ_5	μ_0	Coil magnetic permeability

*IACS: International Annealed Copper Standard (100 % = σ_{Cu})

The mechanical properties of the tube (E, S_1, S_2, S_3, n, ε_0') haven't been changed and are given in **Table 10**.

D.2.3 Other electrical parameters

Transient simulations are done superimposing the current pulse, *i.e.* its peak value I_{peak} and its natural frequency f_n. Pseudo-harmonic approximations are assumed.

Natural frequency: $f_n = 20\ kHz$

Peak current: $I_{peak} = 825\ kA$ (if Z = 30 mm)

Peak current: $I_{peak} = 825*Z[mm]/30\ kA$ (if Z ≠ 30 mm)

Appendix E Experience

E.1 First experiment (*TESTCASE 3*)

E.1.1 The coil geometry

Table 13*: Parameters of the coil geometry of TESTCASE 3.*

Name	Value*	significance
R_{1i}	0.876	internal tube radius
R_{1e}	0.942	external tube radius
$g=g_2$	0.0578	airgap between coil and tube
R_{3i}	1	internal coil radius
R_{3ie}	1.98	intermediate coil radius
R_{3e}	6.6	external coil radius
Z	1.98	useful length of coil
Z_t	3.3	total length of coil

*Values normalized as a function of reference value R_{3i}=1.

E.1.2 The materials

Table 14: *Parameters of the materials (@20°C) of TESTCASE 3.*

Name	Value	significance
σ_1	30 % IACS	Tube electrical conductivity
μ_1	μ_0	Tube magnetic permeability
σ_3	8 % IACS	Coil electrical conductivity
μ_3	μ_0 *to* $5000\mu_0$	Coil magnetic permeability
E	69 GPa	Young modulus of tube
S_1	350 MPa	Johnson Cook coefficient 1
S_2	440 MPa	Johnson Cook coefficient 2
S_3	0.083	Johnson Cook coefficient 3
n	0.43 n.u.	Johnson Cook exponent
ε_0'	1 $\%.s^{-1}$	Reference speed

E.1.3 Other electrical parameters

Transient computations can be done by coupling the electromagnetic model to the mechanical behaviour and the electrical circuit.

The capacitor of the generator is charged such that its maximum initial voltage is: $V_0 = 8500\ V$, *i.e.* maximum energy $E = 25\ kJ$.

The equivalent components of the pulse generator are:

Generator capacitance: $C = 690\ \mu F$

Generator and cables resistance: $R_1 = 2.4\ m\Omega$

Generator and cables inductance: $L_1 = 44\ nH$

The number of modules connected in parallel is 5.

E.2 Second experiment (*TESTCASE 4*)

E.2.1 The coil and field-shaper geometry

Table 15*: Parameters of the coil geometry of TESTCASE 4.*

Name	Value*	significance
R_{1i}	0.823	internal tube radius
R_{1e}	0.926	external tube radius
$g=g_2$	0.0742	airgap between coil and tube
R_{3i}	1	internal field-shaper radius
R_{3ie}	2.292	mid field-shaper radius
R_{3e}	3.292	external field-shaper radius
g_4	0.042	airgap field-shaper - coil
R_{5i}	3.333	internal coil radius
R_{5e}	6.583	external coil radius
Z	1.25	useful length of field-shaper
Z_t	2.5	total length of coil

E.2.2 The materials

Table 16: *Parameters of the materials (@20°C) of TESTCASE 4.*

Name	Value	significance
σ_1	30 % IACS	Tube electrical conductivity
μ_1	μ_0	Tube magnetic permeability
σ_3	46 % IACS**	Field-shaper conductivity
μ_3	μ_0	Field-shaper permeability
σ_5	46 % IACS	Coil electrical conductivity
μ_5	μ_0	Coil magnetic permeability

**(Steel: 8%, CuBe: 25%, Siclanic®: 46% to Cuprofor®: 85%).

The mechanical properties of the Al tube (E, S_1, S_2, S_3, n, ε_0') haven't been changed and are given in **Table 14**.

E.2.3 Other electrical parameters

Transient computations can be done by coupling the electromagnetic model to the mechanical behaviour and the electrical circuit.

The capacitor of the generator is charged such that its initial voltage is: $V_0 = 2500 / 3500 / 4500 / 5500 / 7500\ V$ respectively.

The equivalent components of the pulse generator are:

Generator capacitance: $C = 138\ \mu F / module$

Generator and cables resistance: $R_1 = 12\ m\Omega / module$

Generator and cables inductance: $L_1 = 220\ nH / module$

The maximum number of modules in parallel is 5.